THE JOURNAL OF BIOLOGICAL CHEMISTRY VOL. 284, NO. 34, pp. 22722–22735, August 21, 2009

Formation of the Stable Structural Analog of ADP-sensitive Phosphoenzyme of Ca^{2+}-ATPase with Occluded Ca^{2+} by Beryllium Fluoride

STRUCTURAL CHANGES DURING PHOSPHORYLATION AND ISOMERIZATION[*S]

Received for publication, March 19, 2009, and in revised form, June 24, 2009 Published, JBC Papers in Press, June 26, 2009, DOI 10.1074/jbc.M109.029702

Stefania Danko, Takashi Daiho, Kazuo Yamasaki, Xiaoyu Liu, and Hiroshi Suzuki[1]

From the Department of Biochemistry, Asahikawa Medical College, Asahikawa 078-8510, Japan

As a stable analog for ADP-sensitive phosphorylated intermediate of sarcoplasmic reticulum Ca^{2+}-ATPase $E1PCa_2$·Mg, a complex of $E1Ca_2$·BeF_x, was successfully developed by addition of beryllium fluoride and Mg^{2+} to the Ca^{2+}-bound state, $E1Ca_2$. In $E1Ca_2$·BeF_x, most probably $E1Ca_2$·BeF_3^-, two Ca^{2+} are occluded at high affinity transport sites, its formation required Mg^{2+} binding at the catalytic site, and ADP decomposed it to $E1Ca_2$, as in $E1PCa_2$·Mg. Organization of cytoplasmic domains in $E1Ca_2$·BeF_x was revealed to be intermediate between those in $E1Ca_2$·AlF_4^- ADP (transition state of $E1PCa_2$ formation) and $E2$·BeF_3^-·(ADP-insensitive phosphorylated intermediate $E2P$·Mg). Trinitrophenyl-AMP (TNP-AMP) formed a very fluorescent (superfluorescent) complex with $E1Ca_2$·BeF_x in contrast to no superfluorescence of TNP-AMP bound to $E1Ca_2$·AlF_x. $E1Ca_2$·BeF_x with bound TNP-AMP slowly decayed to $E1Ca_2$, being distinct from the superfluorescent complex of TNP-AMP with $E2$·BeF_3^-, which was stable. Tryptophan fluorescence revealed that the transmembrane structure of $E1Ca_2$·BeF_x mimics $E1PCa_2$·Mg, and between those of $E1Ca_2$·AlF_4^-·ADP and $E2$·BeF_3^-. $E1Ca_2$·BeF_x at low 50–100 μM Ca^{2+} was converted slowly to $E2$·BeF_3^- releasing Ca^{2+}, mimicking $E1PCa_2$·Mg → $E2P$·Mg + $2Ca^{2+}$. Ca^{2+} replacement of Mg^{2+} at the catalytic site at approximately millimolar high Ca^{2+} decomposed $E1Ca_2$·BeF_x to $E1Ca_2$. Notably, $E1Ca_2$·BeF_x was perfectly stabilized for at least 12 days by 0.7 mM lumenal Ca^{2+} with 15 mM Mg^{2+}. Also, stable $E1Ca_2$·BeF_x was produced from $E2$·BeF_3^- at 0.7 mM lumenal Ca^{2+} by binding two Ca^{2+} to lumenally oriented low affinity transport sites, as mimicking the reverse conversion $E2P$·Mg + $2Ca^{2+}$ → $E1PCa_2$·Mg.

Sarcoplasmic reticulum Ca^{2+}-ATPase (SERCA1a),[2] a representative member of the P-type ion transporting ATPases, catalyze Ca^{2+} transport coupled with ATP hydrolysis (Fig. 1) (1–9). The enzyme forms phosphorylated intermediates from ATP or P_i in the presence of Mg^{2+} (10–13). In the transport cycle, the enzyme is first activated by cooperative binding of two Ca^{2+} ions at high affinity transport sites ($E2$ to $E1Ca_2$, steps 1–2) (14) and autophosphorylated at Asp^{351} with MgATP to form the ADP-sensitive phosphoenzyme ($E1P$, step 3), which reacts with ADP to regenerate ATP in the reverse reaction. Upon this $E1P$ formation, the two bound Ca^{2+} are occluded in the transport sites ($E1PCa_2$). Subsequent isomeric transition to the ADP-insensitive form ($E2PCa_2$), *i.e.* loss of ADP sensitivity at the catalytic site, results in rearrangement of the Ca^{2+} binding sites to deocclude Ca^{2+}, reduce the affinity, and open the lumenal gate, thus releasing Ca^{2+} into the lumen ($E2P$, steps 4–5). Finally Asp^{351}-acylphosphate in $E2P$ is hydrolyzed to form the Ca^{2+}-unbound inactive $E2$ state (steps 6 and 7). Mg^{2+} bound at the catalytic site is required as a physiological catalytic cofactor in phosphorylation and dephosphorylation and thus for the transport cycle. The cycle is totally reversible, *e.g.* $E2P$ can be formed from P_i in the presence of Mg^{2+} and absence of Ca^{2+}, and subsequent Ca^{2+} binding at lumenally oriented low affinity transport sites of $E2P$ reverses the Ca^{2+}-releasing step and produces $E1PCa_2$, which is then decomposed to $E1Ca_2$ by ADP.

Various intermediate structural states in the transport cycle were fixed as their structural analogs produced by appropriate ligands such as AMP-PCP (non-hydrolyzable ATP analog) or metal fluoride compounds (phosphate analogs), and their crystal structures were solved at the atomic level (15–22). The three cytoplasmic domains, N, P, and A, largely move and change their organization state during the transport cycle, and the changes are coupled with changes in the transport sites. Most remarkably, in the change from $E1Ca_2$·AlF_4^-·ADP (the transition state for $E1PCa_2$ formation, $E1PCa_2$·ADP·$Mg^{\ddagger}$) to $E2$·BeF_3^- (the ground state $E2P$·Mg) (23–25), the A domain largely rotates by more than 90° approximately parallel to the membrane plane and associates with the P domain, thereby destroying the Ca^{2+} binding sites, and opening the lumenal gate, thus releasing Ca^{2+} into the lumen (see Fig. 2). $E1PCa_2$·Ca·AMP-PN formed by CaAMP-PNP without Mg^{2+} is nearly the same as

* This work was supported by a grant-in-aid for scientific research (B) (to H. S.) from the Ministry of Education, Culture, Sports, Science and Technology of Japan.

[S] The on-line version of this article (available at http://www.jbc.org) contains supplemental Figs. S1–S5.

[1] To whom correspondence should be addressed: Midorigaoka-Higashi, Asahikawa 078-8510, Japan. Tel.: 81-166-68-2350; Fax: 81-166-68-2359; E-mail: hisuzuki@asahikawa-med.ac.jp.

[2] The abbreviations used are: SERCA1a, adult fast-twitch skeletal muscle sarcoplasmic reticulum Ca^{2+}-ATPase; SR, sarcoplasmic reticulum; *E*P, phosphoenzyme; *E*1P, ADP-sensitive phosphoenzyme; *E*2P, ADP-insensitive phosphoenzyme; MOPS, 3-(*N*-morpholino)propanesulfonic acid; TG, thapsigargin; TNP-AMP, 2′(3′)-*O*-(trinitrophenyl)-AMP; $C_{12}E_8$, octaethylene glycol monododecyl ether; N, nucleotide binding; P, phosphorylation; A, actuator; AMP-PNP, adenosine 5′-(β,γ-imido)triphosphate; AMP-PCP, adenosine 5′-(β,γ-methylene)triphosphate; AMP-PN, adenosine 5′-diphosphoramidate.

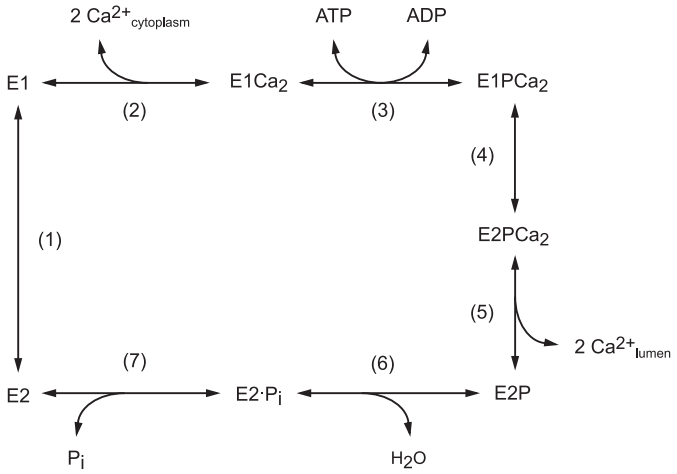

FIGURE 1. **Ca^{2+} transport cycle of Ca^{2+}-ATPase.**

*E*1Ca$_2$·AlF$_4^-$·ADP and *E*1Ca$_2$·CaAMP-PCP in their crystal structures (17, 18, 22).

Despite these atomic structures, yet unsolved is the structure of *E*1PCa$_2$·Mg, the genuine physiological intermediate *E*1PCa$_2$ with bound Mg^{2+} at the catalytic site without the nucleotide. Its stable structural analog has yet to be developed. *E*1PCa$_2$·Mg is the major intermediate accumulating almost exclusively at steady state under physiological conditions. Its rate-limiting isomerization results in Ca^{2+} deocclusion/release producing *E*2P·Mg as a key event for Ca^{2+} transport. In *E*1Ca$_2$·CaAMP-PCP, *E*1Ca$_2$·AlF$_4^-$·ADP, and *E*1PCa$_2$·Ca·AMP-PN, the N and P domains are cross-linked and strongly stabilized by the bound nucleotide and/or Ca^{2+} at the catalytic site, thus they are crystallized (17, 18, 22). Kinetically, *E*1PCa$_2$·Ca formed with CaATP is markedly stabilized due to Ca^{2+} binding at the catalytic Mg^{2+} site, and its isomerization to *E*2P is strongly retarded in contrast to *E*1PCa$_2$·Mg (26, 27). Thus, the bound Ca^{2+} at the catalytic Mg^{2+} site likely produces a significantly different structural state from that with bound Mg^{2+}.

Therefore, it is now essential to develop a genuine *E*1PCa$_2$·Mg analog without bound nucleotide and thereby gain further insight into the structural mechanism in the Ca^{2+} transport process. It is also crucial to further clarify the structural importance of Mg^{2+} as the physiological catalytic cation. In this study, we successfully developed the complex *E*1Ca$_2$·BeF$_x$, most probably *E*1Ca$_2$·BeF$_3^-$, as the *E*1PCa$_2$·Mg analog by adding beryllium fluoride (BeF$_x$) to the *E*1Ca$_2$ state without any nucleotides. For its formation, Mg^{2+} binding at the catalytic site was required and Ca^{2+} substitution for Mg^{2+} was absolutely unfavorable, revealing a likely structural reason for its preference as the physiological cofactor. In *E*1Ca$_2$·BeF$_3^-$, two Ca^{2+} ions bound at the high affinity transport sites are occluded. It was also produced from *E*2·BeF$_3^-$ by lumenal Ca^{2+} binding at the lumenally oriented low affinity transport sites, mimicking *E*2P·Mg + 2Ca^{2+} → *E*1PCa$_2$·Mg. All properties of the newly developed *E*1Ca$_2$·BeF$_3^-$ fulfilled the requirements as the *E*1PCa$_2$·Mg analog, and hence we were able to uncover the hitherto unknown nature of *E*1PCa$_2$·Mg as well as structural events occurring in the phosphorylation and isomerization processes. Also, we successfully found the conditions that perfectly stabilize the *E*1Ca$_2$·BeF$_3^-$ complex.

EXPERIMENTAL PROCEDURES

Preparation of SR Vesicles and Treatment with BeF$_x$, AlF$_x$, and AlF$_x$·ADP—SR vesicles were prepared from rabbit skeletal muscle as described (28). The content of the phosphorylation site in the vesicles determined according to Barrabin *et al.* (29) was 4.49 ± 0.22 nmol/mg of vesicle protein (n = 5). The Ca^{2+}-dependent ATPase activity determined at 25 °C in a mixture containing 5 μg/ml microsomal protein, 1 mM ATP, 1.7 μM A23187, 7 mM MgCl$_2$, 0.1 M KCl, 50 mM MOPS/Tris (pH 7.0), and 0.6 mM CaCl$_2$ with 0.5 mM EGTA (or 2 mM EGTA without added CaCl$_2$) was 1.87 ± 0.14 μmol/min/mg of vesicle protein (n = 3). The Ca^{2+}-ATPase was purified from the vesicles by deoxycholate as described (30, 31). The *E*1Ca$_2$ state ATPase was incubated with fluoride compounds, 2 mM potassium fluoride and 100 μM BeSO$_4$ or AlCl$_3$, at 25 °C for 30 min in the presence of 0.1 mM Ca^{2+}, 15 mM MgCl$_2$, 0.1 M KCl, 30 mM MOPS/Tris buffer (pH 7.0), unless stated otherwise. *E*1Ca$_2$·AlF$_4^-$·ADP was formed by including 50 μM ADP in the above AlF$_x$ incubation mixture as described (32). *E*2·BeF$_3^-$, *E*2·AlF$_4^-$, and *E*2·MgF$_4^{2-}$ were produced as described (23–25).

*Determination of EP—E*P formation was performed with 3 μM [γ-^{32}P]ATP in 100 (or 50) μM Ca^{2+} at 0 °C for 3 s, and terminated by trichloroacetic acid containing carrier P$_i$. The amount of *E*P formed was determined as described previously (28). The background level determined with excess 5 mM EGTA was less than 0.5% of the phosphorylation sites.

Ca^{2+} Binding and Occlusion—^{45}Ca^{2+} binding and occlusion at the transport sites was determined at 25 °C with 2 ml of the SR vesicle mixture (0.2 mg/ml protein) with a 0.45-μm nitrocellulose membrane filter (Millipore) as described (31). In some cases, the vesicles on the filter were washed for 10 s by perfusion with 2 ml of a washing solution containing 5 mM EGTA. The amount of Ca^{2+} bound at the transport sites was obtained by subtracting the nonspecific Ca^{2+} binding level determined as described in the figure legends.

Proteolysis—SR vesicles (0.45 mg/ml protein) were treated at 25 °C with trypsin (0.3 mg/ml) or proteinase K (0.1 mg/ml) as described (23, 24) and as noted in the figure legends. The samples were subjected to Laemmli SDS-PAGE (33) and densitometric analyses of the Coomassie Brilliant Blue R-250-stained gels (23, 24).

Fluorescence Measurements—The TNP-AMP fluorescence and intrinsic tryptophan fluorescence of Ca^{2+}-ATPase (0.06 mg/ml protein) were measured on a RF-5300PC spectrofluorophotometer (Shimadzu, Kyoto, Japan) with excitation and emission wavelengths 408 and 540 nm for TNP-AMP (with band widths 5 and 10 nm), and 290 and 338.4 nm for tryptophan (with bandwidth 1.5 and 5 nm), unless otherwise described (28).

Miscellaneous—Trypsin (L-1-tosylamido-2-phenylethyl chloromethyl ketone-treated) and proteinase K were obtained from Sigma. TNP-AMP was synthesized according to Hiratsuka (34). Protein concentrations were determined by the method of Lowry *et al.* (35) with bovine serum albumin as a standard. Free Ca^{2+} concentrations were calculated by the Calcon program. Data were analyzed by nonlinear regression using the program Origin (Microcal Software, Inc., Northampton,

MA). Three-dimensional models of the enzyme were reproduced by the program VMD (36).

RESULTS

Formation of E1PCa$_2$ Analogs by Fluoride Compounds—The Ca^{2+}-ATPase of SR vesicles in 100 μM Ca^{2+} and 15 mM Mg^{2+} was incubated with beryllium fluoride (BeF$_x$) or aluminum fluoride (AlF$_x$) for 30 min at 25 °C. The ability of *E*P formation from ATP was almost completely lost (actually within 1 min) (Fig. 3), showing the stable complex formation with BeF$_x$ and AlF$_x$. No inhibition occurred with Mg^{2+} and fluoride without beryllium and aluminum (*E1Ca$_2$+(MgF$_x$)*). Thus, MgF$_x$ (MgF$_4^{2-}$) was not able to produce a complex with *E*1Ca$_2$, in contrast to *E*2·MgF$_4^{2-}$ formation from *E*2, the *E*2·P$_i$ product analog in *E*2P hydrolysis (19, 25). This finding agrees with the in-line phosphorylation of *E*1Ca$_2$ to *E*1PCa$_2$ (37), in which there is no state with non-covalently bound P$_i$.

The binding of Mg^{2+} at the catalytic site as a physiological cation is nevertheless required for *E*P formation. Actually in Fig. 3, Mg^{2+} was required for complex formation with BeF$_x$ in 100 μM Ca^{2+}. The apparent Mg^{2+} affinity ($K_{0.5}$ of 5 mM, supplemental Fig. S1) was consistent with that of the catalytic site in phosphorylation from ATP or P$_i$ (*e.g.* Refs. 11, 12, and 38–41). The BeF$_x$-induced inhibition also occurred with Mn^{2+} with apparent affinity ($K_{0.5}$ of 0.6 mM) significantly higher than that of Mg^{2+}, as found in *E*1PCa$_2$ formation and ATP hydrolysis with Mn^{2+} (40, 42).

When Ca^{2+} over millimolar amounts was added in place of Mg^{2+}, the *E*P formation was not inhibited by BeF$_x$ (*BeF$_x$(5 mM Ca)*). Therefore, Ca^{2+} substitution probably at the catalytic Mg^{2+} site abolished complex formation with BeF$_x$. Although CaATP as a substrate and Ca^{2+} bound at the catalytic Mg^{2+} site are able to function for *E*1PCa$_2$ formation (26, 27), Ca^{2+} bound at the catalytic site likely produces different structure from the Mg^{2+}

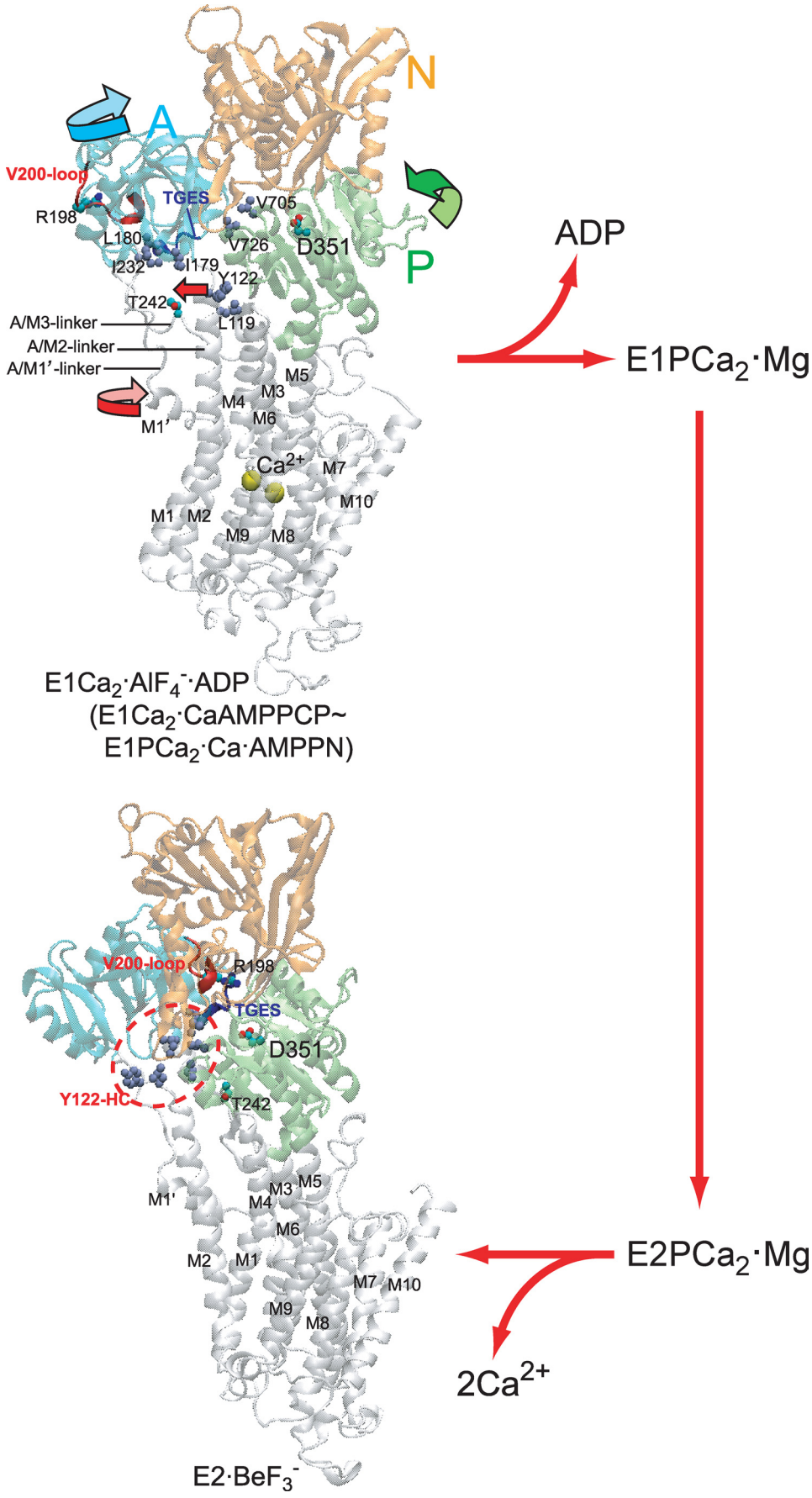

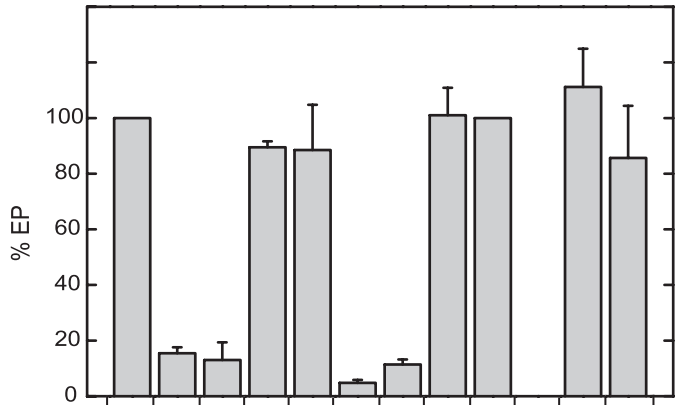

(mM)	E1Ca$_2$	E1Ca$_2$·BeF$_x$ (Mg)	E1Ca$_2$·BeF$_x$ (Mn)	BeF$_x$ (no-Mg/Mn)	BeF$_x$ (5mM Ca)	E1Ca$_2$·AlF$_4^-$ (Mg)	E1Ca$_2$·AlF$_4^-$ (Mn)	AlF$_x$ (no-Mg/Mn)	AlF$_x$ (5mM Ca)		E1Ca$_2$ + (MgF$_x$)	E1Ca$_2$ + (MnF$_x$)
Ca	0.1	0.1	0.1	0.1	5	0.1	0.1	0.1	5		0.1	0.1
Mg	15	15	-	-	-	15	-	-	-		15	-
Mn	-	-	3	-	-	-	3	-	-		-	3
F	-	2	2	2	2	2	2	2	2		2	2
Be	-	0.1	0.1	0.1	0.1	-	-	-	-		-	-
Al	-	-	-	-	-	0.1	0.1	0.1	0.1		-	-

FIGURE 3. **Inhibition of *E*P formation by binding of BeF$_x$ and AlF$_x$ to *E*1Ca$_2$.** The *E*1Ca$_2$ state ATPase of SR vesicles in 0.1 or 5 mM free Ca^{2+} was treated for 30 min at 25 °C with fluoride compounds in the presence of the indicated concentrations of the ligands. Subsequently, the samples were cooled to 0 °C and phosphorylated for 3 s by 3 μM [γ-^{32}P]ATP. The amount of *E*P formed was shown as the percentage of the control value obtained without F$^-$, Be^{2+}, and Al^{3+}. The *E*P formation was not inhibited when the incubations were performed with Be^{2+} or Al^{3+} but without F$^-$. The error bars show the S. D. of five independent experiments.

bound structure (as in fact found, see below). The complex formation of *E*1Ca$_2$ by AlF$_x$ in 100 μM Ca^{2+} also required Mg^{2+} or Mn^{2+} with somewhat higher apparent affinities than those for BeF$_x$-induced complex formation, and was abolished by Ca^{2+} binding at the catalytic site.

Ca^{2+} Binding and Occlusion at Transport Sites—In Fig. 4, Ca^{2+} binding and occlusion in formation of the Ca^{2+}-ATPase complexes with fluoride compounds were determined in 15 mM Mg^{2+} with and without a 10-s EGTA filter washing. In all the cases without washing, Ca^{2+} was bound to the Ca^{2+}-ATPase with high affinities; $K_{0.5}$ at sub-micromolar to millimolar ranges, Hill coefficient ~2, and maximum levels of 9–10 nmol/mg of protein, *i.e.* the stoichiometry of two Ca^{2+} per phosphorylation site (*inset* at 50 μM Ca^{2+}). Therefore, *E*1Ca$_2$·BeF$_x$ and *E*1Ca$_2$·AlF$_4^-$·ADP/*E*1Ca$_2$·AlF$_x$ were produced by cooperative binding of two Ca^{2+} ions at high affinity transport sites. This finding agrees with the property of the sites for Ca^{2+} binding and the resulting enzyme activation for phosphorylation by ATP as nicely demonstrated for the first time by Inesi *et al.* (14). Upon the EGTA washing of *E*1Ca$_2$ that is complexed with BeF$_x$, the two bound Ca^{2+} were not removed, and therefore occluded in the complex as "*E*1Ca$_2$·BeF$_x$." The two Ca^{2+} are occluded also in *E*1Ca$_2$·AlF$_4^-$·ADP and less strongly in *E*1Ca$_2$·AlF$_x$.

Note that the Ca^{2+} affinity became 2–3-fold lower for BeF$_x$ and AlF$_x$. This may be because the Ca^{2+}-free *E*2 state produces *E*2·BeF$_3^-$ and *E*2·AlF$_4^-$ (25), and therefore competes with Ca^{2+} binding for formation of *E*1Ca$_2$·BeF$_x$ and *E*1Ca$_2$·AlF$_x$. On the other hand, the observed ~3-fold Ca^{2+}-affinity increase in formation of *E*1Ca$_2$·AlF$_4^-$·ADP is probably brought about by the fact that ADP together with AlF$_x$ strongly stabilizes the cross-linked N-P domains (17, 18), which is unfavorable for formation of the Ca^{2+}-free *E*2 and *E*2·AlF$_4^-$, because for these structures the A domain should rotate into the opened space between the N and P domains and associate with them (19, 23, 24).

Cytoplasmic Structure in E1Ca$_2$·BeF$_x$ Is Intermediate between Those in E1Ca$_2$·AlF$_4^-$·ADP and E2·BeF$_3^-$—Proteolytic analysis was made to reveal the organization state of the cytoplasmic domains in the newly developed *E*1PCa$_2$·Mg analog *E*1Ca$_2$·BeF$_x$, and to compare with *E*1Ca$_2$·AlF$_4^-$·ADP/*E*1Ca$_2$·AlF$_x$ and *E*2·BeF$_3^-$ (*E*2P·Mg) (see the typical cleavage in supplemental Fig. S2). The initial rate of the "A1" appearance upon cleavage at the T2 site (Arg^{198} on the Val^{200} loop of the A domain) in *E*1Ca$_2$·BeF$_x$ was substantially slower than the rapid cleavage of *E*1Ca$_2$·AlF$_4^-$·ADP and *E*1Ca$_2$·AlF$_x$ as well as *E*1Ca$_2$ (Table 1). The slowed T2 cleavage was also observed when *E*1Ca$_2$·BeF$_x$ was formed with 3 mM Mn^{2+} in place of 15 mM Mg^{2+} (data not shown). Also important was the slow but definitely occurring T2 cleavage in *E*1Ca$_2$·BeF$_x$, in sharp contrast to its complete resistance in *E*2·BeF$_3^-$. Therefore A-P domain organization at the Val^{200} loop in *E*1Ca$_2$·BeF$_x$ is intermediate between those in *E*1Ca$_2$·AlF$_4^-$·ADP/*E*1Ca$_2$·AlF$_x$ and *E*2·BeF$_3^-$.

All complexes were almost completely resistant to proteinase K at the major site of Thr^{242} on the A/M3-linker that produces the "p83" fragment. Therefore, in *E*1Ca$_2$·BeF$_x$, the A domain is rotated perpendicular to the membrane plane from its position in *E*1Ca$_2$ thereby causing the A/M3-linker strain, as in *E*1Ca$_2$·CaAMP-PCP, *E*1Ca$_2$·AlF$_4^-$·ADP (18, 19, 24), and *E*1Ca$_2$·AlF$_x$.

These analyses revealed that in the change *E*1Ca$_2$·AlF$_4^-$·ADP → *E*1Ca$_2$·BeF$_x$ (*i.e.* upon the ADP release from the transition state), the A domain moves, *i.e.* probably rotates to some extent parallel to the membrane plane likely due to the A/M3-linker strain, and thereby Arg^{198} on the Val^{200} loop comes close to the P domain. In the subsequent change, *E*1Ca$_2$·BeF$_x$ → *E*2·BeF$_3^-$, the A domain rotates further (by the A/M3-linker strain as predicted to be motive force (18, 19, 43, 44)) and pro-

FIGURE 2. **Structure of SERCA1a and its change during processing of phosphorylated intermediate.** *E*1Ca$_2$·AlF$_4^-$·ADP (the transition state analog for phosphorylation *E*1PCa$_2$·ADP·Mg‡) and *E*2·BeF$_3^-$ (the ground state *E*2P analog (25)) were obtained from the Protein Data Bank (PDB accession code 1T5T (17) and 2ZBE (21), respectively). Cytoplasmic domains N (nucleotide binding), P (phosphorylation), and A (actuator), and 10 transmembrane helices (M1–M10) are indicated. The *arrows* on the domains, M1′ and M2 (Tyr^{122}) in *E*1Ca$_2$·AlF$_4^-$·ADP, indicate their approximate motions predicted for *E*1PCa$_2$·ADP·Mg‡ → *E*2P·Mg. The phosphorylation site Asp^{351}, TGES^{184} of the A domain, Arg^{198} (tryptic T2 site) on the Val^{200} loop (DPR^{198}AV^{200}NQD) of the A domain, and Thr^{242} (proteinase K site) on the A/M3-linker are shown. Seven hydrophobic residues gather in the *E*2P state to form the Tyr^{122}-hydrophobic cluster (*Y122-HC*); Tyr^{122}/Leu^{119} on the top part of M2, Ile^{179}/Leu^{180}/Ile^{232} of the A domain, and Val^{705}/Val^{726} of the P domain. The overall structure of *E*1Ca$_2$·AlF$_4^-$·ADP is virtually the same as those of *E*1Ca$_2$·CaAMP-PCP and *E*1PCa$_2$·Ca·AMP-PN (17, 18, 22).

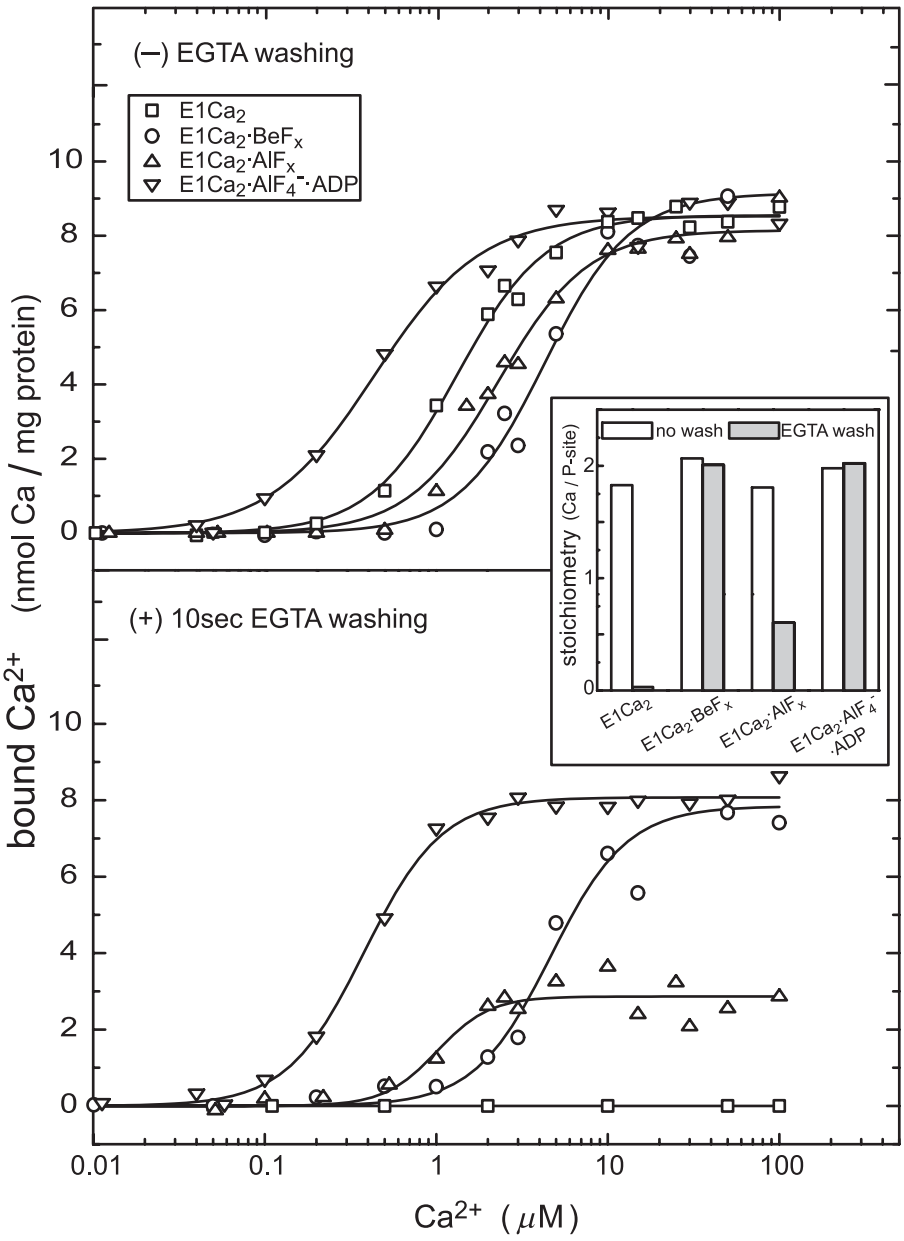

FIGURE 4. **Ca^{2+} binding and occlusion at transport sites.** The *E*1Ca$_2$ state ATPase of SR vesicles in various concentrations of $^{45}Ca^{2+}$ and 15 mM $MgCl_2$ was incubated with BeF_x, AlF_x, and AlF_x·ADP or without these compounds (*E1Ca$_2$*) for 30 min at 25 °C. The amounts of bound (*upper panel*) and occluded (*lower panel*) $^{45}Ca^{2+}$ were determined without and with the perfusion of the membrane filter with a 5 mM EGTA-containing washing solution (without $CaCl_2$ and fluoride compounds otherwise as the above incubation solution). The nonspecific Ca^{2+} binding was determined by including 10 μM thapsigargin before the addition of fluoride compounds, and subtracted. When ADP was used for *E*1Ca$_2$·AlF_4^-·ADP, 5 μM A23187 was included to avoid Ca^{2+} accumulation in the vesicles by ATP produced from ADP due to adenylate kinase in the vesicles. In the *inset*, the stoichiometries of bound Ca^{2+} (*open bars*) and occluded Ca^{2+} (*closed bars*) to the phosphorylation site (P-site) were determined at saturating 50 μM $^{45}Ca^{2+}$. *Solid lines* in the *upper panel* show the least squares fit to the Hill equation. $K_{0.5}$ of Ca^{2+} and Hill coefficients obtained were 1.3 μM and 1.7 (*E1Ca$_2$*), 4.3 μM and 1.7 (*E1Ca$_2$·BeF$_x$*), 2.3 μM and 1.7 (*E1Ca$_2$·AlF$_x$*), and 0.4 μM and 1.4 (*E1Ca$_2$·AlF_4^-·ADP*). In the *lower panel*, the values for E1Ca$_2$·BeF_x and E1Ca$_2$·AlF_4^-·ADP are essentially not altered by EGTA washing (4.7 μM and 1.9, and 0.4 μM and 1.9, respectively).

duces its tight association with the P domain at the Val^{200} loop, mimicking *E*1PCa$_2$·Mg → *E*2P·Mg + 2Ca^{2+}.

Ca^{2+} Ligation at the Catalytic Mg^{2+} Site—The proteolysis further revealed that *E*1Ca$_2$·BeF_x was not produced from *E*1Ca$_2$ in 5 mM Ca^{2+} without Mg^{2+} (*E1Ca$_2$ + 5 mM Ca^{2+} + BeF$_x$* in Table 1), and that *E*1Ca$_2$·BeF_x produced in 15 mM Mg^{2+} and 50–100 μM Ca^{2+} was decomposed to the *E*1Ca$_2$ by 5 mM Ca^{2+} (*E1Ca$_2$·BeF$_x$ + 5 mM Ca^{2+}*), as shown by the rapid cleavage rates at the T2 and proteinase K sites. In *E*1PCa$_2$·Ca and *E*1Ca$_2$·CaAMP-PCP formed in 5 mM Ca^{2+} without Mg^{2+} (Table 1),[3] the T2 site was also rapidly cleaved, in contrast to its substantially slowed cleavage in *E*1Ca$_2$·BeF_x formed with Mg^{2+}. Thus, for organization of the cytoplasmic domains at the T2 site (Arg^{198}), *E*1Ca$_2$·CaAMP-PCP and *E*1PCa$_2$·Ca are very similar to *E*1Ca$_2$·AlF_4^-·ADP, but differ from *E*1Ca$_2$·BeF_x. The close similarity between *E*1Ca$_2$·CaAMP-PCP and *E*1Ca$_2$·AlF_4^-·ADP is in agreement with their nearly same atomic structures and previous observations (17, 18, 45). Also notably, structure *E*1PCa$_2$·Ca·AMP-PN formed by CaAMP-PNP in 10 mM Ca^{2+} without Mg^{2+} (22) is almost identical with those of *E*1Ca$_2$·CaAMP-PCP and *E*1Ca$_2$·AlF_4^-·ADP (see also Table 1).

In *E*1Ca$_2$·CaAMP-PCP and *E*1PCa$_2$·Ca·AMP-PN, the N-P domain cross-linked state is stabilized by Ca^{2+} bound at catalytic Mg^{2+} site I (Asp^{351}/Thr^{353}/Asp^{703} and the phosphate) and by the nucleotide to be nearly identical to the state stabilized with AlF_4^- plus ADP in *E*1Ca$_2$·AlF_4^-·ADP (17, 18, 22). The results on *E*1PCa$_2$·Ca further indicated that such an N-P domain closed state is stabilized solely by site I Ca^{2+} ligation without the nucleotide. The stabilization of this state in *E*1PCa$_2$·Ca is consistent with its markedly retarded isomerization to *E*2P (27), because isomerization requires the A domain rotation into the space between the N and P domains. In *E*1Ca$_2$·BeF_x formed with Mg^{2+} at the catalytic site (site I), such a Ca^{2+} ligation effect is obviously not present. Therefore, the N and P domains are probably more easily separated from each other, and the A domain can rotate into the space between the N and P domains to some extent thus resulting in partial T2 resistance (but not yet as

[3] The proteolytic analysis of *E*1PCa$_2$·Ca was made possible by its markedly retarded decay due to Ca^{2+} ligation at the catalytic site (27) and feedback inhibition by the high lumenal Ca^{2+}. Analysis of *E*1PCa$_2$·Mg formed from MgATP was not feasible because of its very rapid turnover, thus of a very rapid ATP exhaustion.

TABLE 1

Summary of fluorescence changes and proteolysis rates

Maximal TNP-AMP fluorescence intensity at saturating 4 μM TNP-AMP is given as % value of that of *E*2·BeF$_3^-$ without A23187. Tryptophan fluorescence change upon complex formation with the ligand from *E*1Ca$_2$ (or from other state when indicated in parentheses) is shown as % value of the intensity of *E*1Ca$_2$ (see also supplemental Fig. S3*E*). The cleavage rate at the T2 site (Arg^{198}) with trypsin and the digestion rate of the 110-kDa ATPase chain with proteinase K were obtained by the detailed time course analysis in the initial 1 (*T2*) and 30 min (*proteinase K*), and shown as % values of those determined with *E*1Ca$_2$ in 0.1 mM Ca^{2+}. Some of these experiments were done at 0.05 mM Ca^{2+} instead of 0.1 mM, but the results were virtually the same and therefore are represented with 0.1 mM Ca^{2+} for simplicity. It should also be mentioned that the digestion rates in *E*1Ca$_2$ were not altered by 5 or 0.7 mM Ca^{2+} or by A23187 (being 97–101% of the rates of *E*1Ca$_2$ in 0.1 mM Ca^{2+} without A23187), and that the ligand-free *E*2 state was also rapidly digested by trypsin and proteinase K, and TG binding to *E*2 and A23187 did not alter essentially the rapid cleavage rates (Refs. 23–25). The other Ca^{2+}-ATPase complexes were produced under the same buffer conditions as those for *E*1Ca$_2$·BeF$_x$ formation, otherwise as follows and noted below: *E*1Ca$_2$·MgAMP-PCP by 5 mM MgAMP-PCP; *E*1Ca$_2$·CaAMP-PCP by 5 mM CaAMP-PCP; *E*1PCa$_2$·Ca·AMP-PN by 5 mM CaAMP-PNP; *E*1PCa$_2$·Ca by 5 mM CaATP. *E*1Ca$_2$·BeF$_x$ + 5 mM Ca^{2+}, the *E*1Ca$_2$·BeF$_x$ complex was formed in 15 mM Mg^{2+} and 100 μM Ca^{2+} and then incubated with the subsequently added 5 mM Ca^{2+} for 3 h; *E*1Ca$_2$ + 5 mM Ca^{2+} + BeF$_x$, the *E*1Ca$_2$ state ATPase was incubated with BeF$_x$ for 10 min in the presence of 5 mM Ca^{2+} without Mg^{2+}.

ATPase state (→ consequent state, if altered)	Ca^{2+} (mM)/Mg^{2+} (mM)	Relative TNP-AMP fluorescence intensity, see Fig. 5*A* and supplemental Fig. S5	Change in tryptophan fluorescence from *E*1Ca$_2$ (or from another state), supplemental Fig. S3 ↑ increase, ↓ decrease	Relative digestion rate	
				Trypsin (T2), supplemental Fig. S2	Proteinase K, supplemental Fig. S2
	mM	%	*% of E1Ca$_2$ level*	%	
*E*1Ca$_2$	0.1/15	7	(3.27 ↑ from *E*2)	100	100
*E*1Ca$_2$·MgAMP-PCP	0.1/15		0	64	25
*E*1Ca$_2$·CaAMP-PCP	5/0		0.80 ↑	61	9
*E*1Ca$_2$·AlF$_4^-$·ADP	0.1/15		0.84 ↑	65	3
*E*1PCa$_2$·Ca·AMP-PN	5/0		0.77 ↑	65	4
*E*1Ca$_2$·AlF$_x$	0.1/15	7	0	70	10
*E*1PCa$_2$·Ca	5/0		0.89 ↓	80	6
*E*1PCa$_2$·Mg	0.1/15		1.18 ↓		
*E*1Ca$_2$·BeF$_x$	0.1/15	75	1.27 ↓	35	13
*E*1Ca$_2$·BeF$_x$ + 5 mM Ca^{2+} (→ partially *E*1Ca$_2$)	0.1/15 + 5 mM Ca^{2+}	30		70	32
*E*1Ca$_2$ + 5 mM Ca^{2+} + BeF$_x$	5/0	16	0	116	90
*E*2·BeF$_3^-$	0/15	100	(0.66 ↑ from *E*2)	0	0
*E*1Ca$_2$·BeF$_x$ + TG (→ *E*2·BeF$_3^-$(TG))	0.1/15	64	(5.35 ↓ from *E*1Ca$_2$·BeF$_x$)	0	0
*E*2·BeF$_3^-$ + TG (→ *E*2·BeF$_3^-$(TG))	0/15	65	(4.62 ↓ from *E*2·BeF$_3^-$)	0	0
*E*1Ca$_2$·BeF$_x$ + A23187 (→ *E*2·BeF$_3^-$)	0.1/15	100		10	0
*E*2·BeF$_3^-$ + A23187	0/15	100		0	0
*E*1PCa$_2$·Mg (0.7 mM Ca^{2+})	0.7/15		1.19 ↓		
*E*1Ca$_2$·BeF$_x$ (0.7 mM Ca^{2+})	0.7/15	75	1.27 ↓	39	15
*E*1Ca$_2$·BeF$_x$ (0.7 mM Ca^{2+} + A23187)	0.7/15	75		32	8
*E*2·BeF$_3^-$ + 0.7 mM Ca^{2+}	0/15 + 0.7 mM Ca^{2+}	100	(0 from *E*2·BeF$_3^-$)	0	2
*E*2·BeF$_3^-$ + 0.7 mM Ca^{2+} + A23187 (→ *E*1Ca$_2$·BeF$_3^-$)	0/15 + 0.7 mM Ca^{2+}	75		38	16

completely as in *E*2·BeF$_3^-$). As the cause of the Ca^{2+}-induced *E*1Ca$_2$·BeF$_x$ to *E*1Ca$_2$ decomposition, Ca^{2+} replacement of Mg^{2+} at site I altered the domain organization state and made the BeF$_x$ ligation unfavorable (see "Discussion").

TNP-AMP Superfluorescence—TNP-AMP binds to the nucleotide binding site with an extremely high affinity (46–48), and in the *E*2P ground state and its analog *E*2·BeF$_3^-$, the bound TNP-AMP develops its extremely high fluorescence "superfluorescence" (25), which reflects a strongly hydrophobic atmosphere around Asp^{351} (49, 50). On the other hand, it has been controversial whether *E*1PCa$_2$ develops TNP-AMP superfluorescence, mostly because its tight binding to the nucleotide binding site prevents phosphorylation to form *E*1PCa$_2$·Mg, so the TNP-AMP·*E*1PCa$_2$·Mg complex is not formed in significant amounts. Nakamoto and Inesi (47), nevertheless, predicted the development of superfluorescence in *E*1PCa$_2$.

Here, with *E*1Ca$_2$·BeF$_x$ as the *E*1PCa$_2$·Mg analog, we examined the superfluorescence without ATP. In Fig. 5, *A* and *B*, we first formed *E*1Ca$_2$·BeF$_x$ in 15 mM Mg^{2+} and 50 μM Ca^{2+}, then TNP-AMP was added to give a saturating level of 4 μM. *E*1Ca$_2$·BeF$_x$ rapidly developed superfluorescence, and then the fluorescence decreased slowly (much more slowly and extensively at 4 °C).[4] The proteolysis after the loss of superfluorescence revealed that *E*1Ca$_2$·BeF$_x$ was decomposed to *E*1Ca$_2$ (data not shown). Thus, *E*1Ca$_2$·BeF$_x$ develops superfluorescence, and the TNP-AMP binding *per se* causes its decomposition to *E*1Ca$_2$, in sharp contrast to the completely stable *E*2·BeF$_3^-$ even after TNP-AMP binding. The maximum superfluorescence level of *E*1Ca$_2$·BeF$_x$ was slightly lower than that of *E*2·BeF$_3^-$ (Fig. 5, *A-C*), which is the same as that of *E*2P·Mg formed from P$_i$ (25). The results clearly revealed that the atmosphere around Asp^{351} in *E*1Ca$_2$·BeF$_x$ is strongly hydrophobic, similar to *E*2·BeF$_3^-$, although the cytoplasmic domain organization in *E*1Ca$_2$·BeF$_x$ distinctly differs from and did not yet reach the most compactly organized state in *E*2·BeF$_3^-$.

*E*1Ca$_2$·AlF$_x$ as well as *E*2 and *E*1Ca$_2$ did not develop superfluorescence despite high affinity TNP-AMP binding. Therefore the catalytic site in *E*1Ca$_2$·AlF$_x$ is hydrophilic and differs critically from the strongly hydrophobic site in *E*1Ca$_2$·BeF$_x$. Note also that *E*2·AlF$_4^-$ (*E*2-P‡) and *E*2·MgF$_4^{2-}$ (*E*2·P$_i$) do not develop TNP-AMP superfluorescence (25). The superfluorescence therefore develops solely with Ca^{2+}-ATPase complexed with BeF$_x$; *E*1Ca$_2$·BeF$_x$ and *E*2·BeF$_3^-$.

The superfluorescence development of *E*1Ca$_2$·BeF$_x$ in the presence of 15 mM Mg^{2+} and 50 μM Ca^{2+} was rapidly diminished with increasing Ca^{2+} over millimolar concentrations of

[4] The fluorescence level after the decrease of the transient superfluorescence of *E*1Ca$_2$·BeF$_x$ was somewhat higher than the non-superfluorescent low level of TNP-AMP bound to *E*1Ca$_2$ especially at 25 °C. We obtained the results indicating that a small fraction of *E*2·BeF$_3^-$ was produced even in the presence of 50 μM Ca^{2+} (more at 25 than at 4 °C) after the TNP-AMP-induced *E*1Ca$_2$·BeF$_x$ decomposition to *E*1Ca$_2$, and therefore remained somewhat superfluorescence (data not shown).

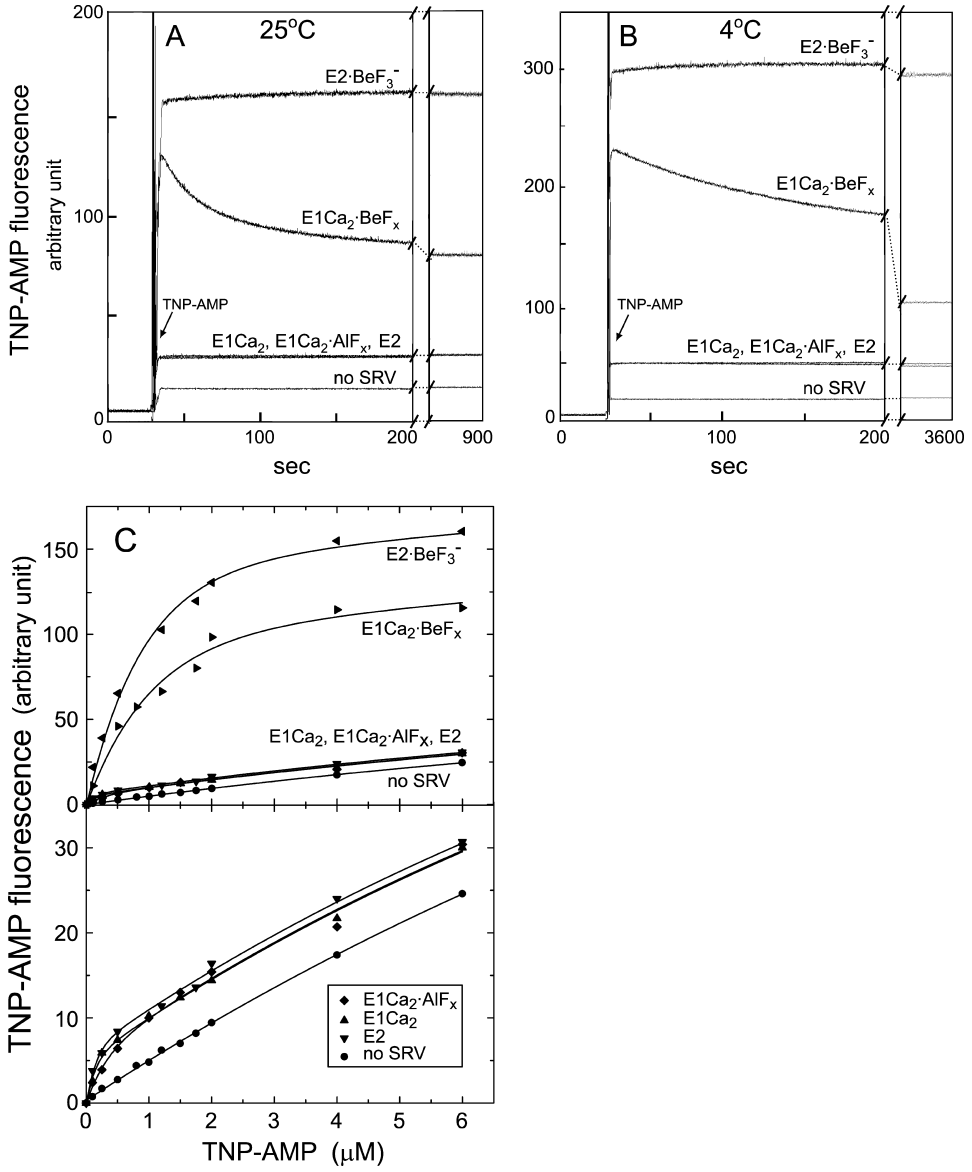

FIGURE 5. **TNP-AMP superfluorescence of *E*1Ca$_2$·BeF$_x$ and *E*2·BeF$_3^-$.** *E*1Ca$_2$·BeF$_x$ and *E*1Ca$_2$·AlF$_x$ were produced in 50 μM Ca^{2+} and 15 mM MgCl$_2$, then at 25 (*A*) and 4 °C (*B*), a small volume of TNP-AMP was added to give saturating 4 μM, and the TNP-AMP fluorescence was followed. The fluorescence of *E*2·BeF$_3^-$ produced with BeF$_x$ in the absence of Ca^{2+}, the *E*1Ca$_2$ and *E*2 states without the fluoride compounds, and without SR vesicles (*no SRV*) were also followed. *C*, the TNP-AMP fluorescence intensities were measured at various concentrations of TNP-AMP at 25 °C, otherwise as described for *A*. For *E*1Ca$_2$·BeF$_x$, the maximum level of transient superfluorescence was determined by extrapolating its decrease to the time of TNP-AMP addition. In the *lower panel* in *C*, the low fluorescence was replotted on the expanded scale. The maximum fluorescence intensities at saturating 4 μM TNP-AMP were obtained by subtracting the background level without TNP-AMP and the level of 4 μM TNP-AMP without the SR vesicles, and given as the relative values in Table 1.

Ca^{2+} (see Fig. 8 and Table 1). Also, inclusion of 5 mM Ca^{2+} without Mg^{2+} in the *E*1Ca$_2$·BeF$_x$ formation mixture abolished the superfluorescence (Table 1). The results agree with the above findings that *E*1Ca$_2$·BeF$_x$ is not produced from and decomposed to *E*1Ca$_2$ by Ca^{2+} ligation at the catalytic Mg^{2+} site (site I).

Transmembrane Domain Structure—The 12 tryptophan residues among 13 in the Ca^{2+}-ATPase are located at the transmembrane region. The tryptophan fluorescence changes in fact reflect the transmembrane domain structural changes, *i.e.* rearrangements of the transmembrane helices upon Ca^{2+} binding to the high affinity transport sites and during the transport cycle (28, 51, 52) as found originally by Dupont and Leigh (53). As summarized in Table 1 with typical fluorescence traces in supplemental Fig. S3, the fluorescence changes were determined at 4 °C upon formation of the *E*1PCa$_2$ analogs by the addition of fluoride compounds to *E*1Ca$_2$ in 15 mM Mg^{2+} and 100 μM Ca^{2+}. *E*1Ca$_2$·BeF$_x$ formation decreased fluorescence by 1.3% very similar to the decrease in *E*1PCa$_2$·Mg formation from *E*1Ca$_2$ by MgATP, *i.e.* in *E*1Ca$_2$·MgATP → *E*1PCa$_2$·Mg (52). In contrast, *E*1Ca$_2$·AlF$_x$ formation did not cause any change. The *E*1Ca$_2$·AlF$_4^-$·ADP formation increased the fluorescence by 0.8%. (F$^-$ alone and ADP alone did not cause any change, except the dilution (F$^-$) and absorption of excitation light (ADP).) Thus the transmembrane structure of *E*1Ca$_2$·BeF$_x$ mimics that of *E*1PCa$_2$·Mg, but those of *E*1Ca$_2$·AlF$_4^-$·ADP and *E*1Ca$_2$·AlF$_x$ differ substantially although the Ca^{2+} ions are occluded at the transport sites (or less strongly in *E*1Ca$_2$·AlF$_x$, Fig. 4). This observation is consistent with the finding in proteolysis and TNP-AMP superfluorescence that organization of the cytoplasmic domains and structure at the catalytic site in *E*1Ca$_2$·BeF$_x$ substantially differ from those in *E*1Ca$_2$·AlF$_4^-$·ADP and *E*1Ca$_2$·AlF$_x$. It is concluded that the transmembrane structure with the occluded Ca^{2+} adopts not simply one state, but changes with the change in the cytoplasmic region during phosphoryl transfer and ADP release (see the diagram of tryptophan fluorescence change in supplemental Fig. S3*E* (with Ref. 54)).

Upon formation of *E*1Ca$_2$·CaAMP-PCP and *E*1PCa$_2$·Ca·AMP-PN by CaAMP-PCP and CaAMP-PNP, respectively, the fluorescence increased by 0.8% equal to that upon *E*1Ca$_2$·AlF$_4^-$·ADP formation (Table 1), in agreement with their essentially identical structures with occluded Ca^{2+} (17, 18, 22, 45). By contrast, the fluorescence did not change upon formation of the *E*1Ca$_2$·MgAMP-PCP, which is the Ca^{2+}-unoccluded state (28, 45), and in rapid equilibrium with *E*1Ca$_2$.

Upon the exclusive accumulation of *E*1PCa$_2$·Ca by CaATP without Mg^{2+}, tryptophan fluorescence decreased by 0.9%, being slightly less than that by formation of *E*1PCa$_2$·Mg and *E*1Ca$_2$·BeF$_x$ (Table 1). Thus in the overall structure,

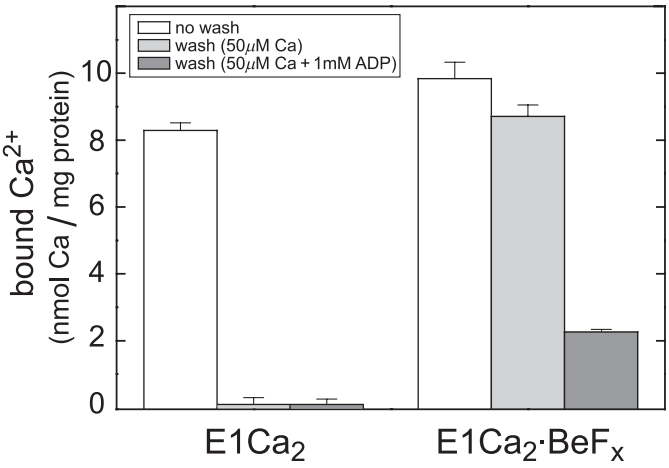

FIGURE 6. **ADP causes the loss of Ca^{2+} occlusion in *E*1Ca$_2$·BeF$_x$.** *E*1Ca$_2$·BeF$_x$ or *E*1Ca$_2$ were produced in 50 μM ^{45}Ca^{2+} and 15 mM Mg^{2+} as described in the legend to Fig. 4, then subjected to membrane filtration without and with perfusion for 20 s by the same buffer containing 50 μM non-radioactive Ca^{2+} (in place of ^{45}Ca^{2+}) with and without 1 mM ADP. The amounts of ^{45}Ca^{2+} specifically bound and occluded in the Ca^{2+}-ATPase were determined by subtracting the nonspecific background level (2.03 ± 0.04 nmol/mg) obtained with the above perfusion without ADP of the *E*1Ca$_2$ state. The error bars show the S. D. of three independent experiments.

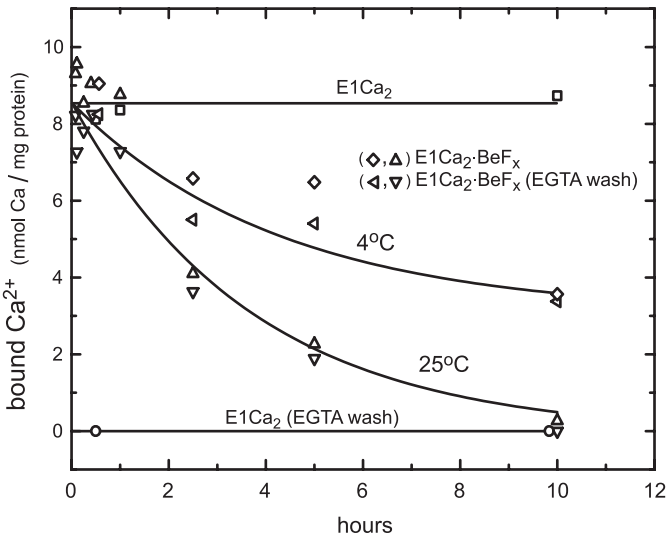

FIGURE 7. **Conversion of *E*1Ca$_2$·BeF$_x$ to *E*2·BeF$_3^-$ with Ca^{2+} release.** The complex *E*1Ca$_2$·BeF$_x$ was produced at 25 °C in 50 μM ^{45}Ca^{2+} and 15 mM MgCl$_2$ as described in the legend to Fig. 4. The complex was then further incubated in the presence of these ligands at 25 and 4 °C for various periods, and the bound ^{45}Ca^{2+} was determined with and without EGTA washing as described in the legend to Fig. 4*A*. In the control, the bound ^{45}Ca^{2+} in *E*1Ca$_2$ without BeF$_x$ was determined.

*E*1PCa$_2$·Ca may be between *E*1Ca$_2$·CaAMP-PCP and *E*1PCa$_2$·Mg (*E*1Ca$_2$·BeF$_x$), and closer to the latter state. Although Ca^{2+} ligation at catalytic Mg^{2+} site I in *E*1PCa$_2$·Ca favors the N-P domain closed state, similar to *E*1Ca$_2$·CaAMP-PCP, the absence of the N-P domain cross-linking nucleotide in *E*1PCa$_2$·Ca likely altered the overall structure slightly.

Upon formation of *E*2·BeF$_3^-$ from *E*2 by BeF$_x$ and Mg^{2+} without Ca^{2+}, the fluorescence increased by 0.7%, mimicking the change upon *E*2P·Mg formation from *E*2 with P$_i$ and Mg^{2+}, and reflecting the opening of the lumenal gate from the closed state (25). As a consequence, the fluorescence of *E*1Ca$_2$·BeF$_x$ was definitely higher by ~1.3% than that of *E*2·BeF$_3^-$, showing their distinct difference in the transmembrane structure. In agreement, the previous kinetic analysis have shown (28) that tryptophan fluorescence decreases by ~1% in the isomerization/Ca^{2+} release, *E*1PCa$_2$·Mg → *E*2P·Mg + 2Ca^{2+}, reflecting the transmembrane structural change from the Ca^{2+}-occluded state to the Ca^{2+}-released and lumenally opened state.

Upon the addition of thapsigargin (TG) to *E*1Ca$_2$·BeF$_x$ and *E*2·BeF$_3^-$, tryptophan fluorescence decreased rapidly by 5.4 and 4.6%, respectively, and reached the level of *E*2·BeF$_3^-$ with bound TG (*E*2·BeF$_3^-$(TG), see Table 1). TNP-AMP superfluorescence (supplemental Fig. S5, *A* and *B*) and proteolysis (Table 1) also demonstrated that *E*1Ca$_2$·BeF$_x$ was converted by TG to *E*2·BeF$_3^-$(TG). Importantly, as described under supplemental Fig. S4, two Ca^{2+} occluded in *E*1Ca$_2$·BeF$_x$ are most likely released into the lumen by the TG-induced structural perturbation and trapped in the lumen by the bound TG, as TG fixes the lumenal gate in the closed state and suppresses Ca^{2+} leakage (16, 55).

E1Ca$_3$·BeF$_x$ Is ADP-sensitive—In Fig. 6, two ^{45}Ca^{2+} occluded in *E*1Ca$_2$·BeF$_x$ were rapidly removed by washing with 1 mM ADP, whereas the occluded ^{45}Ca^{2+} remained completely without ADP. Thus ADP caused the loss of Ca^{2+} occlusion. In agreement, ADP binding to *E*1Ca$_2$·BeF$_x$ increased tryptophan fluorescence to the *E*1Ca$_2$ level, and resulted in the tryptic T2 site cleavage as *E*1Ca$_2$ with bound ADP (data not shown). By contrast, ADP binding to *E*2·BeF$_3^-$ did not alter its structure (data not shown). The ADP-induced decomposition of *E*1Ca$_2$·BeF$_x$ to *E*1Ca$_2$ was also demonstrated with the ADP-induced loss of TNP-AMP superfluorescence, in contrast to normal superfluorescence development in *E*2·BeF$_3^-$ after ADP incubation (data not shown). Thus *E*1Ca$_2$·BeF$_x$ is ADP-sensitive as *E*1PCa$_2$·Mg, and *E*2·BeF$_3^-$ is ADP-insensitive as *E*2P·Mg.

Conversion of E1Ca$_2$·BeF$_x$ to E2·BeF$_3^-$ at 50 μM Ca^{2+}—In Fig. 7, *E*1Ca$_2$·BeF$_x$ was first formed in SR vesicles with BeF$_x$ at 25 °C in 50 μM Ca^{2+} and 15 mM Mg^{2+}, then further incubated at 25 and 4 °C in the presence of these ligands. The amount of bound and occluded Ca^{2+} was lost slowly ($t_{1/2}$ = ~2 h at 25 °C and ~7 h at 4 °C). TNP-AMP superfluorescence (Fig. 8) and tryptic and proteinase K proteolyses (data not shown) revealed that *E*1Ca$_2$·BeF$_x$ turned to *E*2·BeF$_3^-$ with Ca^{2+} loss. Thus *E*1Ca$_2$·BeF$_x$ proceeded its spontaneous slow conversion to *E*2·BeF$_3^-$, as the autoisomerization of *E*1PCa$_2$·Mg to *E*2P·Mg. The Ca^{2+} ions released into the lumen may leak out during such long periods. In *E*1Ca$_2$·AlF$_x$ and *E*1Ca$_2$·AlF$_4^-$·ADP, the amount of bound (occluded) Ca^{2+} was not decreased during the above 10-h incubation at 25 °C (data not shown). The proteolysis showed that these complexes were not converted to the Ca^{2+}-released forms, *E*2·AlF$_4^-$ (*E*2·AlF$_x$) with and without ADP (data not shown). The results indicate that the product state *E*1PCa$_2$·Mg in the phosphoryl transfer acquires the structure ready for autoisomerization to *E*2P·Mg releasing Ca^{2+}, whereas the transition state structure is not yet fully prepared for autoisomerization to the Ca^{2+}-released *E*2P form. Interestingly, as described in supplemental Figs. S4 and S5 (with Refs. 56 and 57), the conversion *E*1Ca$_2$·BeF$_x$ → *E*2·BeF$_3^-$ was markedly accelerated by the transmembrane structural perturbation with hydrophobic reagents such as A23187, lasalocid, and C$_{12}$E$_8$, as

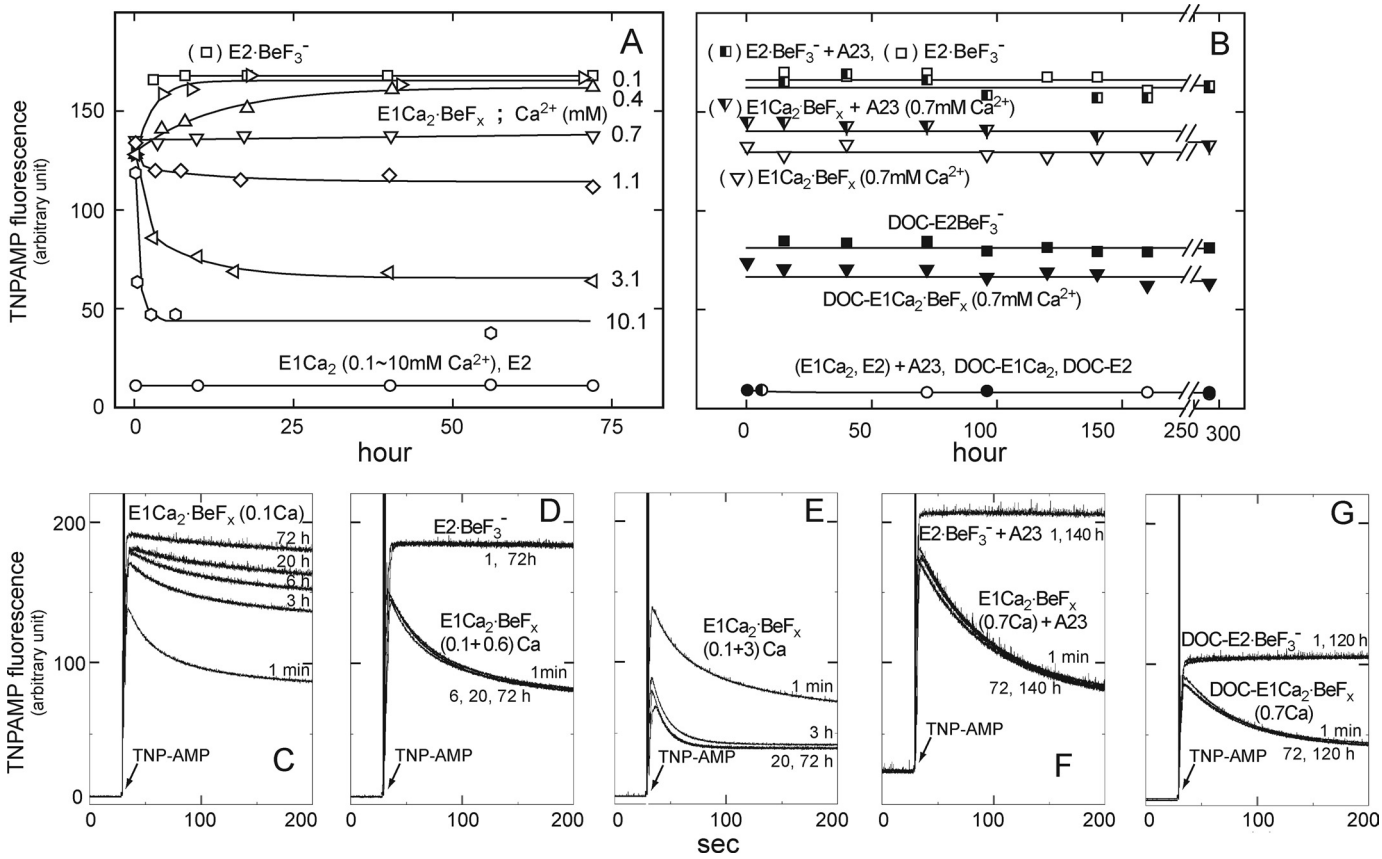

FIGURE 8. **Stability of *E*1Ca$_2$·BeF$_x$ in various Ca^{2+} concentrations.** *A*, *E*1Ca$_2$·BeF$_x$ was first produced in SR vesicles in 0.1 mM Ca^{2+} and 15 mM MgCl$_2$ with BeF$_x$. Subsequently, Ca^{2+} was changed to 0.1 (unchanged), 0.4, 0.7, 1.1, 3.1, and 10.1 mM, and the incubations continued at 25 °C for 72 h. At the indicated periods, the superfluorescence with 4 μM TNP-AMP was examined at 25 °C, and the maximum levels obtained as described in the legend to Fig. 6 are shown. *E*2·BeF$_3^-$ formed without Ca^{2+}, *E*1Ca$_2$ in 0.1–10 mM Ca^{2+}, and *E*2 without Ca^{2+} were also incubated. *B*, in the presence of 0.7 mM Ca^{2+}, *E*1Ca$_2$ in SR vesicles was first incubated with and without 1.2 μM A23187 (*A23*), then BeF$_x$ was added (*E1Ca$_2$·BeF$_x$*). *E*1Ca$_2$·BeF$_x$ (*DOC-E1Ca$_2$·BeF$_x$*) was also produced from *E*1Ca$_2$ in 0.7 mM Ca^{2+} of the Ca^{2+}-ATPase purified and delipidated from SR vesicles by deoxycholate (*DOC*) treatment (30). The incubation was continued for 12 days, otherwise as indicated in *A*. *E*2·BeF$_3^-$ (*E2·BeF$_3^-$*, *DOC-E2·BeF$_3^-$*) without Ca^{2+} and *E*1Ca$_2$ in 0.7 mM Ca^{2+} (*E1Ca$_2$*, *DOC-E1Ca$_2$*) and *E*2 without Ca^{2+} (*E2*, *DOC-E2*) were also incubated. *C–G*, the fluorescence traces upon TNP-AMP addition were shown for the representative samples with incubation periods and Ca^{2+} concentration (mM). Note that at 0.7 mM Ca^{2+}, both with and without A23187, the development of the *E*1Ca$_2$·BeF$_x$ characteristic transient superfluorescence remained perfectly the same for 12 days. By contrast, the transient superfluorescence was converted to the stable and higher superfluorescence characteristic of *E*2·BeF$_3^-$ at 0.1 and 0.4 mM Ca^{2+}, and it was markedly reduced by 3 and 10 mM Ca^{2+} due to decomposition to *E*1Ca$_2$.

well as TG. In contrast, *E*1Ca$_2$·AlF$_x$ and *E*1Ca$_2$·AlF$_4^-$·ADP were resistant against these reagents.

E1Ca$_2$·BeF$_x$ Is Perfectly Stabilized at 0.7 mM Ca^{2+}—As found here, Ca^{2+} binding at high affinity transport sites in *E*1Ca$_2$ is obligatorily required for *E*1Ca$_2$·BeF$_x$ formation, whereas millimolar high Ca^{2+} (Ca^{2+} ligation at the catalytic Mg^{2+} site I) decomposes this complex to *E*1Ca$_2$. Furthermore, *E*1Ca$_2$·BeF$_x$ at 50 μM Ca^{2+} is spontaneously and slowly converted to *E*2·BeF$_x$ releasing Ca^{2+}, and the conversion is markedly accelerated by transmembrane perturbation with hydrophobic reagents such as $C_{12}E_8$ and A23187 (see supplemental materials). The results showed that *E*1Ca$_2$·BeF$_x$ as the *E*1PCa$_2$·Mg analog possesses the structure prepared for its isomerization to *E*2·BeF$_3^-$ with Ca^{2+} release as *E*1PCa$_2$·Mg → *E*2P·Mg + 2Ca^{2+}. On the other hand, it is essential for crystallographic studies to find conditions to perfectly stabilize the *E*1Ca$_2$·BeF$_x$ complex. In Fig. 8*A*, *E*1Ca$_2$·BeF$_x$ was first formed in 0.1 mM Ca^{2+} and 15 mM Mg^{2+}, then further incubated with various concentrations of Ca^{2+} with and without A23187. The structural state was monitored by TNP-AMP superfluorescence (Fig. 8), proteolysis, and tryptophan fluorescence (see Table 1 for representative data). Then we successfully found that Ca^{2+} at a very narrow concentration range, 0.7 mM, perfectly stabilizes *E*1Ca$_2$·BeF$_x$ and maintains this complex for at least 12 days at 25 °C (and 4 °C) even in the presence of A23187. The ^{45}Ca^{2+} binding measurements on *E*1Ca$_2$·BeF$_x$ in 0.7 mM ^{45}Ca^{2+} demonstrated that two Ca^{2+} ions are bound and occluded in this complex (Fig. 9*A*).

The perfectly stable *E*1Ca$_2$·BeF$_x$ was produced from *E*1Ca$_2$ even in the presence of A23187 if 0.7 mM Ca^{2+} was included before BeF$_x$ addition (Fig. 8, *B* and *F*, and Table 1). Also, *E*1Ca$_2$·BeF$_x$ was successfully produced with the Ca^{2+}-ATPase purified from SR vesicles by delipidation with deoxycholate (30); in this case again, by including 0.7 mM Ca^{2+} before BeF$_x$ addition. *E*1Ca$_2$·BeF$_x$ thus produced with the purified and delipidated Ca^{2+}-ATPase was perfectly stable at least for 12 days at 4 and 25 °C in 0.7 mM Ca^{2+} (Fig. 8, *B* and *G*, at 25 °C).

E1Ca$_2$·BeF$_3^-$ Is Produced from E2·BeF$_3^-$ by Lumenal Ca^{2+} Binding—We successfully found also that *E*1Ca$_2$·BeF$_x$ (*E*1Ca$_2$·BeF$_3^-$) can be produced from *E*2·BeF$_3^-$ by lumenal Ca^{2+} binding, as mimicking the lumenal Ca^{2+}-induced reverse transition, *E*2P·Mg + 2Ca^{2+} → *E*1PCa$_2$·Mg. In Fig. 10, we added

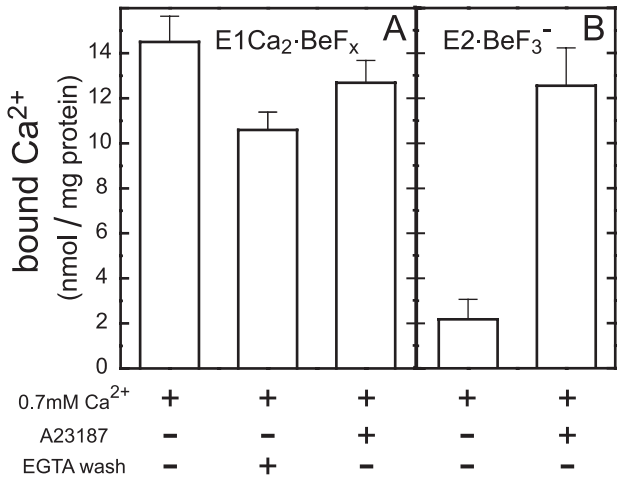

FIGURE 9. **Two Ca^{2+} are bound in $E1Ca_2{\cdot}BeF_x$ formed from $E1Ca_2$ and from $E2{\cdot}BeF_3^-$ at 0.7 mM Ca^{2+}.** *A*, SR vesicles in 0.7 mM $^{45}Ca^{2+}$ were incubated with BeF_x in the absence or presence of 5 μM A23187, otherwise as described in the legend to Fig. 4. The amount of bound Ca^{2+} was obtained with subtraction of the background level (10.1 ± 0.5 nmol/mg (n = 6)) determined by EGTA washing the vesicles incubated without BeF_x and A23187. The occluded Ca^{2+} was determined by EGTA washing in the absence of A23187 and by subtraction of the background level. (Here the determination of occluded Ca^{2+} in A23187 by EGTA washing was not feasible, because in the absence of (or even in 0.1 mM) Ca^{2+}, A23187 converts $E1Ca_2{\cdot}BeF_x$ very rapidly to $E2{\cdot}BeF_3^-$ releasing Ca^{2+} (supplemental Figs. 4 and 5). *B*, $E2{\cdot}BeF_3^-$ was first produced in SR vesicles without A23187 and Ca^{2+}. Subsequently, the samples were diluted 10 times with the buffer containing $^{45}CaCl_2$ and BeF_x with and without 5 μM A23187, to give 0.7 mM $^{45}Ca^{2+}$ and the same buffer conditions as in *A*. At 15 s after dilution, the amount of bound $^{45}Ca^{2+}$ was determined without EGTA washing and by subtracting the nonspecific Ca^{2+} binding (1.0 ± 0.1 nmol/mg (n = 6)) determined by EGTA washing the sample incubated without BeF_x and A23187.

various concentrations of Ca^{2+} to $E2{\cdot}BeF_3^-$ formed in SR vesicles in 15 mM Mg^{2+} without Ca^{2+} in the presence and absence of A23187, then at 10 s after Ca^{2+} addition the structural state was examined by TNP-AMP superfluorescence. With increasing Ca^{2+} to 0.7 mM in the presence of A23187, the stable superfluorescence of $E2{\cdot}BeF_3^-$ was converted to the transient and slightly lower superfluorescence characteristic of $E1Ca_2{\cdot}BeF_x$ with $K_{0.5}$ of 0.4 mM Ca^{2+} and a Hill coefficient of 4 (Fig. 10, *A* and *D*). A further Ca^{2+} increase in the millimolar range caused the marked loss of superfluorescence with $K_{0.5}$ of 1.7 mM and a Hill coefficient of 1 (Fig. 10, *B* and *D*). The proteolysis also clearly showed that $E2{\cdot}BeF_3^-$ was converted to $E1Ca_2{\cdot}BeF_x$ by 0.7 mM Ca^{2+} in A23187 (Table 1), and this complex was further decomposed to $E1Ca_2$ by 10 mM Ca^{2+} (data not shown). In Fig. 9*B*, two $^{45}Ca^{2+}$ were shown to be bound producing $E1Ca_2{\cdot}BeF_x$, when 0.7 mM $^{45}Ca^{2+}$ was added to $E2{\cdot}BeF_3^-$ in the presence of A23187. In contrast, in the absence of A23187, $E2{\cdot}BeF_3^-$ was neither converted to $E1Ca_2{\cdot}BeF_x$ nor decomposed to $E1Ca_2$ even at 10 mM Ca^{2+} (Figs. 9*B* and 10, *C* and *E*, and Table 1 (proteolysis at 0.7 mM Ca^{2+})).

The results demonstrated that $E1Ca_2{\cdot}BeF_x$, most probably $E1Ca_2{\cdot}BeF_3^-$, was produced from $E2{\cdot}BeF_3^-$ by the lumenal Ca^{2+} binding at the lumenally oriented low affinity transport sites, and further that Ca^{2+} substitution of Mg^{2+} at the catalytic site in $E1Ca_2{\cdot}BeF_3^-$ produced from $E2{\cdot}BeF_3^-$ caused its decomposition to $E1Ca_2$, therefore as the change $E2{\cdot}BeF_3^- + 2Ca^{2+} \rightarrow E1Ca_2{\cdot}BeF_3^- \rightarrow E1Ca_2$. Note that Mg^{2+} bound at the catalytic site in $E2P{\cdot}Mg$ is occluded, whereas it is not and therefore is exchangeable in $E1PCa_2{\cdot}Mg$ (42). Thus, these two distinctly different states of the ligated Mg^{2+} at the catalytic site (site I) in $E2P{\cdot}Mg$ and $E1PCa_2{\cdot}Mg$ are obviously mimicked here by the respective analogs $E2{\cdot}BeF_3^-$ and $E1Ca_2{\cdot}BeF_3^-$. The perfect stabilization of $E1Ca_2{\cdot}BeF_3^-$ achieved by 0.7 mM Ca^{2+} (Fig. 10) obviously involves lumenal Ca^{2+} binding and prevention of the Ca^{2+} release into the lumen. The stabilization by 0.7 mM Ca^{2+} in the absence of A23187 is probably due to Ca^{2+} moved passively into the vesicle lumen during the long incubation periods. All these findings show that the forward and reverse transition, $E1PCa_2{\cdot}Mg \leftrightarrow E2P{\cdot}Mg + 2Ca^{2+}$, is mimicked by the forward and reverse conversion, $E1Ca_2{\cdot}BeF_3^- \leftrightarrow E2{\cdot}BeF_3^- + 2Ca^{2+}$.

It is of interest to note the Hill coefficient of 4 in the lumenal Ca^{2+}-induced reverse conversion, $E2{\cdot}BeF_3^- + 2Ca^{2+} \rightarrow E1Ca_2{\cdot}BeF_3^-$ at 0.1–0.7 mM Ca^{2+} in Fig. 10*A*. This might be indicative of the existence of lumenal Ca^{2+} access sites in addition to transport sites and their possible cooperative involvement in lumenal Ca^{2+} access to the transport sites. In fact, two such sites besides the two transport sites have been suggested by the kinetics and protein-chemical study on the lumenal loops (58, 59).

DISCUSSION

Formation of $E1Ca_2{\cdot}BeF_3^-$—As a structural analog of the physiological intermediate $E1PCa_2{\cdot}Mg$, the $E1Ca_2{\cdot}BeF_x$ complex was successfully produced by BeF_x binding to the $E1Ca_2$ state Ca^{2+}-ATPase and from $E2{\cdot}BeF_3^-$ by lumenal Ca^{2+} binding to the lumenally oriented low affinity transport sites. All the revealed properties of $E1Ca_2{\cdot}BeF_x$ met the requirements for the $E1PCa_2{\cdot}Mg$ analog; *i.e.* two Ca^{2+} occluded at the transport sites, Mg^{2+} bound (but not occluded) at the catalytic site, the ADP-released but still ADP-sensitive state, and its isomerization to the ADP-insensitive Ca^{2+}-released state $E2P{\cdot}Mg$ ($E2{\cdot}BeF_3^-$) and reversal by lumenal Ca^{2+} binding, $E1PCa_2{\cdot}Mg \leftrightarrow E2P{\cdot}Mg + 2Ca^{2+}$.

Furthermore, the coordination chemistry of beryllium fluoride, actually BeF_3^-, fulfills the requirement of $E1Ca_2{\cdot}BeF_x$ as the $E1PCa_2{\cdot}Mg$ analog. In chemistry, beryllium fluoride compounds are known to adopt tetrahedral geometry with the Be-F 1.55-Å bond length, thereby making them strictly isomorphous to the tetrahedral phosphate group (60). Moreover, because of the high charge density due to the small size, beryllium is able to coordinate the aspartate-oxygen in addition to F^-. The -O-BeF_3^- thus produced with Asp^{351}-oxygen in fact possesses the tetrahedral geometry superimposable with the covalently bound phosphate at the aspartate, as actually seen in $E2{\cdot}BeF_3^-$, the $E2P{\cdot}Mg$ ground-state analog (21, 22, 25). MgF_4^{2-} also possesses the tetrahedral geometry, but magnesium is not able to be coordinated directly with the Asp^{351}-oxygen, as seen in $E2{\cdot}MgF_4^{2-}$, the $E2{\cdot}P_i$ analog. AlF_4^- in $E1Ca_2{\cdot}AlF_4^-{\cdot}ADP$ and $E2{\cdot}AlF_4^-$ (17, 18, 20) (or AlF_3 in some cases in the haloacid dehalogenase superfamily (61)) possesses planar geometry, in which Asp^{351}-oxygen and ADP β-phosphate or the hydrolytic water ($E2{\cdot}AlF_4^-$) coordinate the aluminum at apical positions producing the bipyramidal structure superimposable to the penta-coordinated phosphorus in the transition state of in-line phosphoryl transfer $E1PCa_2{\cdot}ADP{\cdot}Mg^{\ddagger}$ and acylphosphate hydrolysis $E2\text{-}P{\cdot}Mg^{\ddagger}$. Thus all chemical properties of the P_i ana-

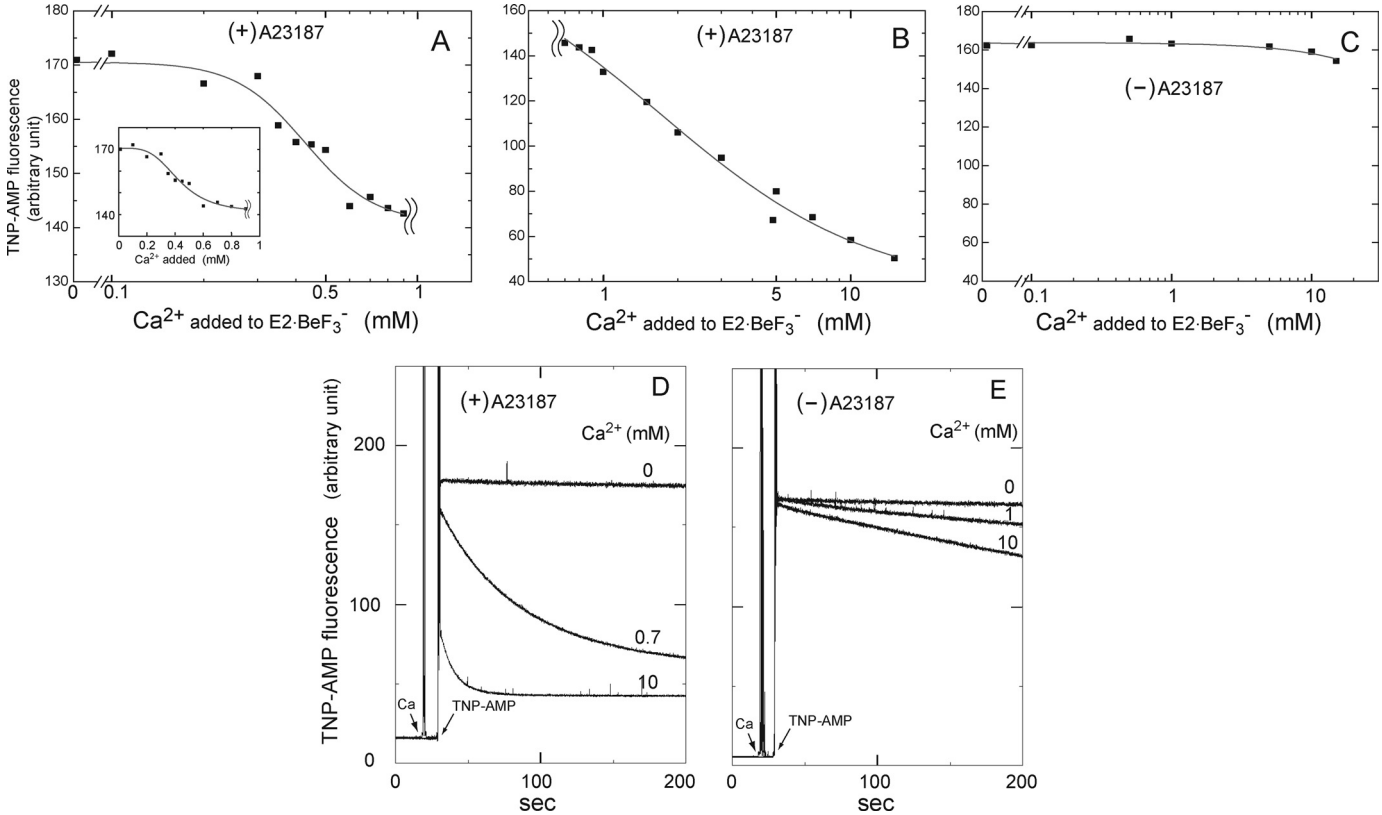

FIGURE 10. **Formation of *E*1Ca$_2$·BeF$_3^-$ from *E*2·BeF$_3^-$ by lumenal Ca^{2+} binding.** *E*2·BeF$_3^-$ was first produced in SR vesicles with BeF$_x$ in the presence and absence of 1.2 μM A23187 at 25 °C in 0.5 mM EGTA, 15 mM $MgCl_2$, 0.1 M KCl, and 30 mM MOPS/Tris (pH 7.0). Then a small volume of $CaCl_2$ was added to give various Ca^{2+} concentrations as indicated. At 10 s after this Ca^{2+} addition, TNP-AMP fluorescence was monitored with 4 μM TNP-AMP. In *A* and *B*, the maximum intensity in the presence of A23187 was plotted in semi-log scale at 0–0.9 mM Ca^{2+} (*A*) and 0.7–15 mM Ca^{2+} (*B*). Note also the different scales in the *ordinates*. The *inset* in *A* is the linear plot at 0–0.9 mM Ca^{2+} to clearly show the saturation of the first phase of the Ca^{2+}-dependent change, *i.e.* the formation of *E*1Ca$_2$·BeF$_3^-$ from *E*2·BeF$_3^-$. In *C*, the maximum superfluorescence intensity in the absence of A23187 was plotted at 0–15 mM Ca^{2+}. In *D* and *E*, the traces of superfluorescence development upon TNP-AMP addition in the presence of A23187 (*D*) or its absence (*E*) were shown at the representative Ca^{2+} concentrations (0, 0.7 or 1.0, and 10 mM). *Solid lines* in *A* and *B* show the least squares fit to the Hill equation. Apparent Ca^{2+} affinity ($K_{0.5}$) and Hill coefficients at 0–0.9 mM Ca^{2+} are 0.43 mM and 3.8 with the intensity decrease from 170 to 142, and those at Ca^{2+} over 0.7 mM are 1.7 mM and 1.0 with a further intensity decrease to 36.

logs agree with the conclusion that *E*1Ca$_2$·BeF$_x$ is the analog for *E*1PCa$_2$·Mg, and BeF$_x$ is most probably BeF$_3^-$, *i.e.* *E*1Ca$_2$·BeF$_3^-$.

Here note that the replacement of phosphate with BeF$_3^-$ produces stabilization of the *E*1PCa$_2$·Mg structure with the same geometry of BeF$_3^-$ as phosphate, and therefore probably with the same binding residues for them within the catalytic site. The *E*1Ca$_2$·BeF$_3^-$ stability is likely brought about by the specific chemical nature of fluoride. Namely, it possesses a significantly higher electronegativity than oxygen (actually the highest among all atoms) and a small size, therefore producing stronger BeF$_3^-$ binding in the catalytic site and fixing the intermediate structure.

Structure of E1Ca$_2$·BeF$_3^-$—Then with the newly developed *E*1Ca$_2$·BeF$_3^-$, we explored its structural properties and uncovered the hitherto unknown nature of the physiological intermediate *E*1PCa$_2$·Mg and structural changes during the phosphoryl transfer/ADP release and subsequent *E*P isomerization/Ca^{2+} release. The observed proteinase K resistance of Thr^{242} on the A/M3-linker revealed that, in *E*1PCa$_2$·Mg (*E*1Ca$_2$·BeF$_3^-$) the A domain is already rotated perpendicular to the membrane plane from the position in *E*1Ca$_2$, thereby bringing up its junction with the A/M3-linker and imposing a strain on this linker, similarly to *E*1Ca$_2$·AlF$_4^-$·ADP and *E*1Ca$_2$·CaAMP-PCP (17, 18). As described for the *E*1Ca$_2$·CaAMP-PCP structure (18), the A/M3-linker strain, *i.e.* the A domain perpendicular rotation is brought about by bending the P domain due to binding of the phosphate moiety and Ca^{2+} at the catalytic site (Mg^{2+}-site I, Asp^{351}/Thr^{353}/Asp^{703}) on the P domain (see Figs. 4 and 5 in Ref. 18).[5] Our results revealed that such a strained state is achieved even without the N-P domain cross-linking nucleotide but solely with BeF$_3^-$ and Mg^{2+} binding at the catalytic site, and therefore remains in *E*1PCa$_2$·Mg after ADP release.

The strain of the A/M3-linker thus imposed has been predicted with the atomic structure (18, 19) to function as a motive force for the A domain rotation parallel to the membrane in the *E*1P to *E*2P isomerization. The partial resistance at T2 site Arg^{198} in *E*1Ca$_2$·BeF$_3^-$ (as compared with the rapid cleavage in *E*1Ca$_2$·CaAMP-PCP/*E*1Ca$_2$·AlF$_4^-$·ADP and *E*1Ca$_2$·AlF$_x$) further indicated that in *E*1PCa$_2$·Mg, the A domain is already likely

[5] As depicted in Figs. 4 and 5 by Toyoshima *et al.* (18) for the change *E*1Ca$_2$ → *E*1Ca$_2$·CaAMP-PCP, the top part of the first half of the P domain (Pβ1–Pβ4) moves together as a result of γ-phosphate and Ca^{2+} (Mg^{2+}) binding, because Thr^{353} just above Pβ1 coordinates to both ligands. Furthermore, Pβ5 twists upon binding of Ca^{2+} (Mg^{2+}) because of the coordination by Asp^{703}, which causes Pα5–Pα7 tilting. Thus the P domain is bent. This bending causes the perpendicular A domain rotation because the P7 helix moves upwards and tilts so that Gly^{156}–Lys^{158} on the A domain is brought up as they are in contact with Ala^{725}–Val^{726} on top of the P7 helix.

rotated parallel to the membrane to some extent from the position in *E*1Ca$_2$·MgATP*/*E*1PCa$_2$·ADP·Mg‡. Thus, the A/M3-linker strain is likely functioning for this partial A domain rotation during the phosphoryl transfer/ADP release to produce *E*1PCa$_2$·Mg, and further for the large and complete rotation to achieve the tight A-P domain association at Arg^{198} on the Val^{200} loop in the Ca^{2+}-released state *E*2P·Mg (*E*2·BeF$_3^-$). The A-P domain interaction at the Val^{200} loop is actually critical for formation of the proper Ca^{2+}-released structure, *E*2P·Mg and its analog *E*2·BeF$_3^-$ (25, 62, 63).

Here, it is of interest to note that residues Asp^{351}, Thr^{353}, and Asp^{703} ligating Mg^{2+} and phosphate will come more proximate to each other during *E*1PCa$_2$·ADP·Mg‡ → *E*1PCa$_2$·Mg + ADP (*E*1Ca$_2$·AlF$_4^-$·ADP/*E*1Ca$_2$·AlF$_x$ → *E*1Ca$_2$·BeF$_x$). As a consequence, a further P domain bending and more strain for the A/M3-linker will likely be induced by this coordination-chemical change, thereby contributing to inducing the A domain rotations during *E*1PCa$_2$·Mg formation and subsequent isomerization to *E*2PCa$_2$·Mg (besides the release of the N-P domain cross-linking nucleotide ADP). In any case, our results show that *E*1PCa$_2$·Mg (*E*1Ca$_2$·BeF$_3^-$) as the product of the phosphorylation reaction acquires the structure ready for isomerization and Ca^{2+} deocclusion/release (*i.e.* ready for the large A domain rotation to produce *E*2P·Mg (*E*2·BeF$_3^-$)), whereas the transition state structure in the phosphorylation (*E*1Ca$_2$·AlF$_4^-$·ADP and *E*1Ca$_2$·AlF$_x$) is not yet fully prepared. Note again that the *E*1PCa$_2$·Mg structure before such motions for its isomerization to *E*2P·Mg is stabilized with replacement of phosphate with BeF$_3^-$ in *E*1Ca$_2$·BeF$_3^-$.

Important also, we found that the Ca^{2+}-occluded transmembrane structure adopts not simply one state, but will proceed through changes during the phosphoryl transfer and ADP release to form *E*1PCa$_2$·Mg (see supplemental Fig. S3*E*). The structural change is probably coupled with the above described motions of the P and A domains (more bending and rotation) during this process. In the subsequent Ca^{2+} deocclusion/release in *E*1PCa$_2$·Mg → *E*2P·Mg + 2Ca^{2+}, the transmembrane structure changes further (52), which was also clearly mimicked here in the change *E*1Ca$_2$·BeF$_3^-$ → *E*2·BeF$_3^-$. Thus, the structures of the transmembrane domain as well as the cytoplasmic domains in *E*1Ca$_2$·BeF$_3^-$ (*E*1PCa$_2$·Mg) are intermediate between those of *E*1Ca$_2$·AlF$_4^-$·ADP (*E*1PCa$_2$·ADP·Mg‡) and *E*2·BeF$_3^-$ (*E*2P·Mg).

Mg^{2+} as Physiological Catalytic Cation—Important questions regarding the *E*1Ca$_2$·BeF$_3^-$ structure are why Ca^{2+} coordination at the catalytic Mg^{2+} site (site I, Asp^{351}/Thr^{353}/Asp^{703}) is absolutely unfavorable for *E*1Ca$_2$·BeF$_3^-$ formation, and why the Mg^{2+}-coordinated structure *E*1Ca$_2$·BeF$_3^-$ differs from Ca^{2+}-coordinated *E*1PCa$_2$·Ca, *E*1Ca$_2$·CaAMP-PCP, and *E*1PCa$_2$·Ca·AMP-PN structures as well as from *E*1Ca$_2$·AlF$_4^-$·ADP/*E*1Ca$_2$·AlF$_x$, especially in A domain positioning. These questions may be relevant to the questions of why forward isomerization of *E*1PCa$_2$·Ca to *E*2P is markedly retarded in contrast to *E*1PCa$_2$·Mg and thus why Mg^{2+} is preferred as the catalytic cation. In stringent coordination chemistry, the coordination distance of Mg^{2+} is shorter than Ca^{2+}, typically by 0.2 Å (*e.g.* 2.1 *versus* 2.3 Å (64, 65)). As a consequence, in the case of *E*1Ca$_2$·CaAMP-PCP, the distance between the γ-phosphate and Asp^{351}-oxygen becomes 3.24 Å, being greater by 0.3 Å than that predicted in *E*1Ca$_2$·MgAMP-PCP. Therefore MgAMP-PCP (MgATP) binding would result in steric clash, and *E*1Ca$_2$·CaAMP-PCP is more stable than *E*1Ca$_2$·MgAMP-PCP, and therefore has less tendency to decompose to *E*1Ca$_2$ (also in the forward direction to the *E*P formation and its decay in the case of *E*1Ca$_2$·CaATP) (45). In *E*1Ca$_2$·BeF$_3^-$ formed here with Mg^{2+}, the direct coordination between Asp^{351} and the beryllium and their proximate positioning would probably favor the closely positioned ligand residues (Thr^{353}/Asp^{703}/Asp^{351}) for BeF$_3^-$ and Mg^{2+} but not for Ca^{2+}. Therefore Ca^{2+} substitution of Mg^{2+} probably disrupted the precise geometry and decomposed the *E*1Ca$_2$·BeF$_3^-$ complex. Also, a possible difference in the coordination number might be involved; Mg^{2+} prefers definitely six, whereas Ca^{2+} can accommodate seven or eight ligands (65–69).

Furthermore, the difference in A domain positioning between the Mg^{2+}-coordinated state *E*1Ca$_2$·BeF$_3^-$ and the Ca^{2+}-coordinated states may be reasonably understood by the consequence of the stringent coordination chemistry. Namely, because the shorter coordination distance of Mg^{2+}, P domain bending, and the resulting A domain rotation perpendicular to the membrane will be greater in the Mg^{2+}-coordinated state. Therefore the strain of the A/M3-linker and A domain rotation parallel to the membrane will be more in the Mg^{2+} state *E*1Ca$_2$·BeF$_x$. In this context, it is also reasonable that *E*1PCa$_2$·Mg is more rapidly isomerized to *E*2P with less energy barrier for the large A domain rotation, in contrast to the retarded isomerization in *E*1PCa$_2$·Ca that is stabilized by the likely conformational inadequacy. Here note that the cause of the *E*1PCa$_2$·Ca stabilization is obviously different from that of *E*1PCa$_2$·Mg stabilization produced by replacement of phosphate with BeF$_3^-$ (see the above discussion for *E*1Ca$_2$·BeF$_3^-$ stabilization).

Previously it was documented (45, 64, 70) that destabilization of the non-covalent complex *E*1Ca$_2$·MgATP by Mg^{2+} (as found with MgAMP-PCP *versus* CaAMP-PCP) together with stabilization of the transition state by Mg^{2+} (as found with *E*1Ca$_2$·AlF$_4^-$·ADP bound Mg^{2+} at both sites I and II) leads to a decrease of the activation energy and a rapid phosphoryl transfer. As another critical reason for Mg^{2+} preference for catalysis, we predict here by exploring the property of the *E*1Ca$_2$·BeF$_x$ that the Mg^{2+} bound at the catalytic site produces the proper *E*1PCa$_2$ structure, which is ready for rapid transition to *E*2P in this rate-limiting process of the transport cycle.

Hydrophobic Catalytic Site in E1Ca$_2$·BeF$_3^-$—The microenvironment around Asp^{351} in *E*1PCa$_2$·Mg was further predicted by TNP-AMP superfluorescence in *E*1Ca$_2$·BeF$_3^-$ to be strongly hydrophobic and thus a closed state, and this will become even more in the change *E*1PCa$_2$·Mg → *E*2P·Mg + 2Ca^{2+} (*E*1Ca$_2$·BeF$_3^-$ → *E*2·BeF$_3^-$). The observed distinct difference between *E*1Ca$_2$·BeF$_3^-$ and *E*2·BeF$_3^-$ (transient *versus* stable and slightly higher superfluorescence) is probably ascribed to the distinct difference in the organization state of cytoplasmic domains. The superfluorescence, nevertheless, developed solely in the Ca^{2+}-ATPase complexed with beryllium fluoride, *E*1Ca$_2$·BeF$_3^-$ and *E*2·BeF$_3^-$ (*E*2P·Mg), but no development in *E*1Ca$_2$·AlF$_x$ and in *E*2·AlF$_4^-$ and *E*2·MgF$_4^{2-}$ (25). Therefore, the

hydrophobic closed catalytic site is accomplished by the direct coordination and close proximity of the beryllium with Asp^{351}-oxygen and by the specific coordination of the tetrahedral -O-BeF_3^-, *i.e.* Asp^{351}-acylphosphate within the catalytic site. This is obviously not the case in AlF_4^- (the penta-coordinated phosphorus of the transition states) and MgF_4^{2-} (non-covalently bound P_i), thus in these states, the catalytic site is more accessible to nonspecific water molecules.

Whether *E*1PCa$_2$·Mg develops the superfluorescence had been controversial. In addition to the obvious problem of TNP-AMP competition against ATP for phosphorylation, the observed TNP-AMP-induced decomposition of *E*1Ca$_2$·BeF_3^- further revealed that the *E*1PCa$_2$·Mg structure may be similarly disrupted rapidly by TNP-AMP binding, therefore making it virtually impossible to examine the superfluorescence development in *E*1PCa$_2$·Mg. The TNP-AMP-induced *E*1Ca$_2$·BeF_3^- decomposition might have occurred by means of a similar structural change as the ADP-induced one, *i.e.* disruption of the cytoplasmic domain organization and possible BeF_3^- release. The most important conclusion here is that the hydrophobic and closed property of the phosphorylated catalytic site both in *E*1PCa$_2$·Mg and *E*2P·Mg may be requisite to avoid a possible attack of nonspecific water molecules on the Asp^{351}-acylphosphate thus accomplishing Ca^{2+} release into the lumen and energy coupling.

Formation of E1Ca$_2$·BeF_3^- from E2·BeF_3^- and Perfect Stabilization of E1Ca$_2$·BeF_3^-—E1Ca$_2$·BeF_3^- was produced also from *E*2·BeF_3^- by binding two lumenal Ca^{2+} to the lumenally oriented low affinity transport sites at 0.7 mM Ca^{2+} and 15 mM Mg^{2+}, as mimicking the reverse transition *E*2P·Mg + 2Ca^{2+} → *E*1PCa$_2$·Mg. At the critical concentration of 0.7 mM Ca^{2+} in 15 mM Mg^{2+}, *E*1Ca$_2$·BeF_3^- is perfectly stabilized without decomposition to *E*1Ca$_2$ or conversion to *E*2·BeF_3^-. The perfect *E*1Ca$_2$·BeF_3^- stabilization is obviously achieved by preventing Ca^{2+} release into the lumen and by avoiding the absolutely unfavorable Ca^{2+} substitution of Mg^{2+} in site I at the most appropriately balanced concentrations of Ca^{2+} and Mg^{2+}. As noted in the last paragraph under "Results," stabilization of *E*1Ca$_2$·BeF_3^- might possibly involve lumenal Ca^{2+} access at the putative lumenal gating sites besides the transport sites. If this is the case, the gate-opening and Ca^{2+} release into the lumen takes place when the lumenal Ca^{2+} is low enough to avoid the possible lumenal Ca^{2+} access to the gate.

Integrated Picture of EP Processing—Recently, we successfully identified and trapped for the first time the intermediate state *E*2PCa$_2$·Mg, ADP-insensitive *E*P with two Ca^{2+} occluded at transport sites, by elongating the A/M1′-linker (71), and revealed that the proper length of this linker is critical for inducing structural changes for Ca^{2+} deocclusion and release from *E*2PCa$_2$·Mg. This dependence on the length of the linker is probably because the length controls the extent of strain between the A domain and M1′, which causes motions of the cytoplasmic A and P domains thereby transmitting the structural signal to the transmembrane transport sites. In trapped *E*2PCa$_2$·Mg, the A domain is already largely rotated, and A-P domain associations at Val^{200} and TGES^{184} loops are already produced, although the interaction network is not produced properly at the Tyr^{122}-hydrophobic cluster (71), which is critical for Ca^{2+} deocclusion/release and *E*2P hydrolysis (72–74). In the Ca^{2+}-released *E*2P·Mg, this cluster is formed from seven residues of the A (Ile^{179}/Leu^{180}/Ile^{232}) and P (Val^{705}/Val^{726}) domains and the top part of M2 (Leu^{119}/Tyr^{122}) (see Fig. 2).

The results indicated that the successive structural changes take place as follows: in *E*1PCa$_2$·Mg → *E*2PCa$_2$·Mg, the A domain rotates largely (further from the position in *E*1PCa$_2$·Mg) into the space between the N and P domains and docks onto the Asp^{351}-acylphosphate of the P domain, thereby causing loss of ADP sensitivity and also the strain of the A/M1′-linker (because the A domain is brought above the P domain). The strain thus imposed will cause inclinations of the A and P domains and the connected M2 and M4/M5 thereby rearranging the helices to destroy Ca^{2+} sites and open the lumenal gate thus to release Ca^{2+}. Upon these motions, the Tyr^{122}-hydrophobic cluster is produced from the inclined A and P domains and M2. Hence, interactions at this cluster and at the Val^{200} loop stabilize the Ca^{2+}-released structure *E*2P·Mg, and also produce the catalytic site for the acylphosphate hydrolysis to occur after Ca^{2+} release, ensuring energy coupling (63, 72–74). Atomic level structural studies of *E*1Ca$_2$·BeF_3^- as *E*1PCa$_2$·Mg and the trapped intermediate state *E*2PCa$_2$·Mg will contribute to further understanding of *E*P processing, Ca^{2+} handling, and *E*2P hydrolysis.

Acknowledgment—We thank Dr. Chikashi Toyoshima, University of Tokyo, for helpful discussions.

REFERENCES

1. Hasselbach, W., and Makinose, M. (1961) *Biochem. Z.* **333,** 518–528
2. Ebashi, S., and Lipmann, F. (1962) *J. Cell Biol.* **14,** 389–400
3. Inesi, G., Sumbilla, C., and Kirtley, M. E. (1990) *Physiol. Rev.* **70,** 749–760
4. Møller, J. V., Juul, B., and le Maire, M. (1996) *Biochim. Biophys. Acta* **1286,** 1–51
5. MacLennan, D. H., Rice, W. J., and Green, N. M. (1997) *J. Biol. Chem.* **272,** 28815–28818
6. McIntosh, D. B. (1998) *Adv. Mol. Cell. Biol.* **23A,** 33–99
7. Toyoshima, C., and Inesi, G. (2004) *Annu. Rev. Biochem.* **73,** 269–292
8. Toyoshima, C. (2008) *Arch. Biochem. Biophys.* **476,** 3–11
9. Toyoshima, C. (2009) *Biochim. Biophys. Acta* **1793,** 941–946
10. Yamamoto, T., and Tonomura, Y. (1968) *J. Biochem.* **64,** 137–145
11. de Meis, L., and Masuda, H. (1974) *Biochemistry* **13,** 2057–2062
12. Masuda, H., and de Meis, L. (1973) *Biochemistry* **12,** 4581–4585
13. Kanazawa, T., and Boyer, P. D. (1973) *J. Biol. Chem.* **248,** 3163–3172
14. Inesi, G., Kurzmack, M., Coan, C., and Lewis, D. E. (1980) *J. Biol. Chem.* **255,** 3025–3031
15. Toyoshima, C., Nakasako, M., Nomura, H., and Ogawa, H. (2000) *Nature* **405,** 647–655
16. Toyoshima, C., and Nomura, H. (2002) *Nature* **418,** 605–611
17. Sørensen, T. L., Møller, J. V., and Nissen, P. (2004) *Science* **304,** 1672–1675
18. Toyoshima, C., and Mizutani, T. (2004) *Nature* **430,** 529–535
19. Toyoshima, C., Nomura, H., and Tsuda, T. (2004) *Nature* **432,** 361–368
20. Olesen, C., Sørensen, T. L., Nielsen, R. C., Møller, J. V., and Nissen, P. (2004) *Science* **306,** 2251–2255
21. Toyoshima, C., Norimatsu, Y., Iwasawa, S., Tsuda, T., and Ogawa, H. (2007) *Proc. Natl. Acad. Sci. U.S.A.* **104,** 19831–19836
22. Olesen, C., Picard, M., Winther, A. M., Gyrup, C., Morth, J. P., Oxvig, C., Møller, J. V., and Nissen, P. (2007) *Nature* **450,** 1036–1042
23. Danko, S., Daiho, T., Yamasaki, K., Kamidochi, M., Suzuki, H., and Toyoshima, C. (2001) *FEBS Lett.* **489,** 277–282
24. Danko, S., Yamasaki, K., Daiho, T., Suzuki, H., and Toyoshima, C. (2001) *FEBS Lett.* **505,** 129–135

25. Danko, S., Yamasaki, K., Daiho, T., and Suzuki, H. (2004) *J. Biol. Chem.* **279,** 14991–14998
26. Shigekawa, M., Wakabayashi, S., and Nakamura, H. (1983) *J. Biol. Chem.* **258,** 8698–8707
27. Wakabayashi, S., and Shigekawa, M. (1987) *J. Biol. Chem.* **262,** 11524–11531
28. Nakamura, S., Suzuki, H., and Kanazawa, T. (1994) *J. Biol. Chem.* **269,** 16015–16019
29. Barrabin, H., Scofano, H. M., and Inesi, G. (1984) *Biochemistry* **23,** 1542–1548
30. Meissner, G., and Fleischer, S. (1974) *Methods Enzymol.* **32,** 475–481
31. Kubota, T., Daiho, T., and Kanazawa, T. (1993) *Biochim. Biophys. Acta* **1163,** 131–143
32. Troullier, A., Girardet, J. L., and Dupont, Y. (1992) *J. Biol. Chem.* **267,** 22821–22829
33. Laemmli, U. K. (1970) *Nature* **227,** 680–685
34. Hiratsuka, T. (1982) *Biochim. Biophys. Acta* **719,** 509–517
35. Lowry, O. H., Rosebrough, N. J., Farr, A. L., and Randall, R. J. (1951) *J. Biol. Chem.* **193,** 265–275
36. Humphrey, W., Dalke, A., and Schulten, K. (1996) *J. Mol. Graph.* **14,** 33–38
37. Webb, M. R., and Trentham, D. R. (1981) *J. Biol. Chem.* **256,** 4884–4887
38. Hasselbach, W., Fassold, E., Migala, A., and Rauch, B. (1981) *Fed. Proc.* **40,** 2657–2661
39. González, D. A., Ostuni, M. A., Lacapère, J. J., and Alonso, G. L. (2006) *Biophys. Chem.* **124,** 27–34
40. Yamada, S., and Ikemoto, N. (1980) *J. Biol. Chem.* **255,** 3108–3119
41. Kanazawa, T. (1975) *J. Biol. Chem.* **250,** 113–119
42. Ogurusu, T., Wakabayashi, S., and Shigekawa, M. (1991) *J. Biochem.* **109,** 472–476
43. Möller, J. V., Lenoir, G., Marchand, C., Montigny, C., le Maire, M., Toyoshima, C., Juul, B. S., and Champeil, P. (2002) *J. Biol. Chem.* **277,** 38647–38659
44. Holdensen, A. N., and Andersen, J. P. (2009) *J. Biol. Chem.* **284,** 12258–12265
45. Picard, M., Toyoshima, C., and Champeil, P. (2005) *J. Biol. Chem.* **280,** 18745–18754
46. Watanabe, T., and Inesi, G. (1982) *J. Biol. Chem.* **257,** 11510–11516
47. Nakamoto, R. K., and Inesi, G. (1984) *J. Biol. Chem.* **259,** 2961–2970
48. Dupont, Y., Chapron, Y., and Pougeois, R. (1982) *Biochem. Biophys. Res. Commun.* **106,** 1272–1279
49. de Meis, L., Martins, O. B., and Alves, E. W. (1980) *Biochemistry* **19,** 4252–4261
50. Dupont, Y., and Pougeois, R. (1983) *FEBS Lett.* **156,** 93–98
51. Champeil, P., Le Maire, M., Moller, J. V., Riollet, S., Guillain, F., and Green, N. M. (1986) *FEBS Lett.* **206,** 93–98
52. Suzuki, H., and Kanazawa, T. (1995) *J. Biol. Chem.* **270,** 3089–3093
53. Dupont, Y., and Leigh, J. B. (1978) *Nature* **273,** 396–398
54. Obara, M., Suzuki, H., and Kanazawa, T. (1988) *J. Biol. Chem.* **263,** 3690–3697
55. Inesi, G., Lewis, D., Toyoshima, C., Hirata, A., and de Meis, L. (2008) *J. Biol. Chem.* **283,** 1189–1196
56. Murphy, A. J., and Coll, R. J. (1993) *J. Biol. Chem.* **268,** 23307–23310
57. Lakowitz, J. R. (1983) *Principles of Fluorescence Spectroscopy*, Plenum Press, New York
58. Myung, J., and Jencks, W. P. (1994) *Biochemistry* **33,** 8775–8785
59. Webb, R. J., Khan, Y. M., East, J. M., and Lee, A. G. (2000) *J. Biol. Chem.* **275,** 977–982
60. Petsko, G. A. (2000) *Proc. Natl. Acad. Sci. U.S.A.* **97,** 538–540
61. Wang, W., Cho, H. S., Kim, R., Jancarik, J., Yokota, H., Nguyen, H. H., Grigoriev, I. V., Wemmer, D. E., and Kim, S. H. (2002) *J. Mol. Biol.* **319,** 421–431
62. Daiho, T., Suzuki, H., Yamasaki, K., Saino, T., and Kanazawa, T. (1999) *FEBS Lett.* **444,** 54–58
63. Kato, S., Kamidochi, M., Daiho, T., Yamasaki, K., Gouli, W., and Suzuki, H. (2003) *J. Biol. Chem.* **278,** 9624–9629
64. Picard, M., Jensen, A. M., Sørensen, T. L., Champeil, P., Møller, J. V., and Nissen, P. (2007) *J. Mol. Biol.* **368,** 1–7
65. Peeraer, Y., Rabijns, A., Collet, J. F., Van Schaftingen, E., and De Ranter, C. (2004) *Eur. J. Biochem.* **271,** 3421–3427
66. Stokes, D. L., and Green, N. M. (2003) *Annu. Rev. Biophys. Biomol. Struct.* **32,** 445–468
67. Yang, W., Lee, H. W., Hellinga, H., and Yang, J. J. (2002) *Proteins Struct. Funct. Genet.* **47,** 344–356
68. Shannon, R. D. (1976) *Acta Crystallogr. Sect. A* **32,** 751–767
69. Falke, J. J., Drake, S. K., Hazard, A. L., and Peersen, O. B. (1994) *Q. Rev. Biophys.* **27,** 219–290
70. Suzuki, H., Nakamura, S., and Kanazawa, T. (1994) *Biochemistry* **33,** 8240–8246
71. Daiho, T., Yamasaki, K., Danko, S., and Suzuki, H. (2007) *J. Biol. Chem.* **282,** 34429–34447
72. Yamasaki, K., Daiho, T., Danko, S., and Suzuki, H. (2004) *J. Biol. Chem.* **279,** 2202–2210
73. Wang, G., Yamasaki, K., Daiho, T., and Suzuki, H. (2005) *J. Biol. Chem.* **280,** 26508–26516
74. Yamasaki, K., Wang, G., Daiho, T., Danko, S., and Suzuki, H. (2008) *J. Biol. Chem.* **283,** 29144–29155